




## Article – Gregory Yu. Ivanyuk memorial issue

# U–Pb geochronology of calcite carbonatites and jacupirangite from the Guli alkaline complex, Polar Siberia, Russia

Ekaterina P. Reguir<sup>1\*</sup> , Ekaterina B. Salnikova<sup>2</sup>, Panseok Yang<sup>1</sup>, Anton R. Chakhmouradian<sup>1</sup>, Maria V. Stifeeva<sup>2</sup>, Irina T. Rass<sup>3</sup> and Aleksandr B. Kotov<sup>2</sup>

<sup>1</sup>Department of Geological Sciences, University of Manitoba, 125 Dysart Road, Winnipeg, MB, R3T 2N2, Canada; <sup>2</sup>Institute of Precambrian Geology and Geochronology, Russian Academy of Sciences, St. Petersburg, 199034, Russia; and <sup>3</sup>Institute of Geology of Ore Deposits, Petrography, Mineralogy and Geochemistry, Moscow, 119017, Russia

### Abstract

This work is the first *in situ* U–Pb geochronological study of perovskite and calcic garnet (andradite) from the Guli complex in the Maimecha–Kotuy alkaline province (Polar Siberia, Russia). The U–Pb isotopic compositions of perovskite from contact zones of the two carbonatite stocks (Southern and Northern) and from jacupirangite separating the stocks were determined by laser-ablation inductively-coupled-plasma mass-spectrometry (LA-ICPMS) and isotope-dilution thermal-ionisation mass-spectrometry (ID-TIMS). The LA-ICPMS and ID-TIMS data for perovskite from the Northern carbonatite stock are in good agreement, yielding <sup>206</sup>Pb/<sup>238</sup>U ages of 250.4 ± 1.1 Ma and 249 ± 2 Ma, respectively. These ages are also within the analytical uncertainty from the ID-TIMS results for perovskite from jacupirangites (250 ± 1 Ma). The LA-ICPMS results for perovskite from the Southern carbonatite stock indicate its somewhat older age (255.3 ± 2.4 Ma), implying the possibility of small-volume mantle magmatism predating the eruption of the Siberian flood basalts at ca. 252–251 Ma. This interpretation is supported by reports of pre-flood magmatism elsewhere in eastern Siberia. Andradite crystals from the contact between the Southern stock and metasomatised melilitolite were analysed by ID-TIMS. These measurements are inconclusive (247 ± 6 Ma) and could not be used to constrain further the timing of carbonatitic magmatism in the southern part of the complex. The present contribution also presents a refined methodology for LA-ICPMS geochronological studies of perovskite with elevated levels of common lead, and addresses some of the problems with previously proposed calibration standards.

**Keywords:** U–Pb geochronology, LA-ICPMS, ID-TIMS, perovskite, andradite, Guli complex, carbonatites, jacupirangite

(Received 10 February 2021; accepted 3 June 2021; Accepted Manuscript published online: 9 June 2021; Guest Associate Editor: Anatoly Zaitsev)

### Introduction

Perovskite (CaTiO<sub>3</sub>) is a common accessory phase in silica-undersaturated igneous rocks, including clinopyroxenites, carbonatites, nephelinites, melilitic rocks, ultramafic lamprophyres and kimberlites (e.g. Chakhmouradian and Mitchell, 1997, 2000; Tappe *et al.*, 2006; Chakhmouradian *et al.*, 2013). Owing to its capacity to concentrate U, Th, rare earth elements (REE), Sr and high-field-strength elements (in particular, Nb and Ta), this mineral has been used widely as a petrogenetic indicator and robust geochronological tool (e.g. Heaman, 1989; Kinny *et al.*, 1997, 1999; Hamilton *et al.*, 2003; Paton *et al.*, 2007; Donnelly *et al.*, 2012; Chakhmouradian *et al.*, 2013; Heaman *et al.*, 2015; Stamm *et al.*, 2018). Since the late 1980s, geochronological studies of perovskite have generally relied on mass-spectrometry techniques, which are capable of providing high-precision results for a

small quantity of material (Stamm *et al.*, 2018; Heaman *et al.*, 2019). Early work utilised isotope-dilution thermal-ionisation mass spectrometry (ID-TIMS) and sensitive high-resolution ion-microprobes (Heaman, 1989; Smith *et al.*, 1989; Ireland *et al.*, 1990; Kinny *et al.*, 1997). In the past 20 years, a considerable effort has been made to develop *in situ* perovskite age determination techniques, including laser-ablation inductively-coupled mass spectrometry (LA-ICPMS) (e.g. Cox and Wilton, 2006; Batumike *et al.*, 2008; Reguir *et al.*, 2010) and secondary-ion mass-spectrometry (Li *et al.*, 2010; Donnelly *et al.*, 2012). The major advantages of LA-ICPMS are its relatively low cost (both infrastructure and operational), expedience, minimal requirements for sample preparation, and the capability for *in situ* measurements at a spatial resolution of 20–30 μm. This capability enables a greater level of control over the material being analysed relative to ID-TIMS. The greatest challenges of LA-ICPMS perovskite geochronology are the lack of well-characterised matrix-matched calibration standards and <sup>204</sup>Pb–<sup>204</sup>Hg interference (Reguir *et al.*, 2010). Perovskite from the Ice River alkaline complex (Canada) has been proposed as a calibration standard for U–Pb radiometric age determination (Heaman, 2009). It is also noteworthy here that the overwhelming majority of the available geochronological data on perovskite are for groundmass crystals from

\*Author for correspondence: Ekaterina P. Reguir, Email: [Ekaterina.Reguir@umanitoba.ca](mailto:Ekaterina.Reguir@umanitoba.ca)  
This paper is part of a thematic set 'Alkaline Rocks' in memory of Dr Gregory Yu. Ivanyuk

**Cite this article:** Reguir E.P., Salnikova E.B., Yang P., Chakhmouradian A.R., Stifeeva M.V., Rass I.T. and Kotov A.B. (2021) U–Pb geochronology of calcite carbonatites and jacupirangite from the Guli alkaline complex, Polar Siberia, Russia. *Mineralogical Magazine* 85, 469–483. <https://doi.org/10.1180/mgm.2021.53>

kimberlites (Smith *et al.*, 1989; Heaman *et al.*, 2015; Donnelly *et al.*, 2012; Stamm *et al.*, 2018; Tappe *et al.*, 2018, to name a few), whereas publications on other rock types – in particular, alkaline-ultramafic intrusions with carbonatites – are very limited (Srivastava *et al.*, 2005; Cox and Wilton, 2006; Heaman, 2009; Reguir *et al.*, 2010).

In comparison with perovskite, Ca-Fe-Ti garnets [ $\text{Ca}_3(\text{Fe,Ti,Zr,Mg})_2(\text{Si,Fe,Al})_3\text{O}_{12}$ ] are a relatively new U–Pb geochronometer, whose full potential remains yet to be fully explored (Deng *et al.*, 2017; Salnikova *et al.*, 2018, 2019; Yang *et al.*, 2018; Stifeeva *et al.*, 2020). The principal advantage of calcic garnets over perovskite is their wider distribution across a spectrum of igneous and contact-metamorphic rocks. In alkaline complexes, calcic garnets are a fairly common accessory or, in some cases, a major mineral in melteigites, ijolites, nephelinites, melilitolites, syenites and, to a lesser extent, carbonatites. These minerals crystallise in a different  $a_{\text{SiO}_2} - f_{\text{O}_2}$  regime relative to perovskite (Rass and Dubrovinskii, 1997) and, thus, can provide valuable complementary information on the timing of alkaline magmatism.

In the present work, we determined the age of perovskite in calcite carbonatites and jacupirangite from the Guli alkaline-ultramafic complex (Polar Siberia, Russia) using ID-TIMS and LA-ICPMS U–Pb techniques, and explored the possibility of using the Ice River perovskite as a calibration standard for age determination using LA-ICPMS. Perovskite is a common accessory phase at Guli, but its geochronology has not been explored to date. In addition, we used ID-TIMS to determine the U–Pb age of andradite from a perovskite-free metasomatic paragenesis at the contact between calcite carbonatite and melilitolite.

## Geological Setting

The Guli alkaline-ultramafic complex is part of the Maimecha-Kotuy Alkaline Province, which is one of the world's largest manifestations of intracontinental alkaline magmatism related to the eruption of the Siberian Traps at the Permian–Triassic boundary (Augland *et al.*, 2019 and references therein). The complex is located at the northern margin of the Siberian Platform (Fig. 1a), bordered by the Yenisey-Khatanga Trough, which developed synchronously with the trap volcanism and evolved into a marginal basin towards the end of the Triassic (Afanasenkov *et al.*, 2016). The Guli complex has an exposed area of 470 km<sup>2</sup> and in its north-northwestern part, is overlain by Mesozoic–Cenozoic sedimentary sequences of the Yenisey-Khatanga Trough (Yegorov, 1989, 1991). According to unpublished gravimetric and aeromagnetic data, the northern, buried portion of the complex represents a series of blocks subsided by as much as 4 km towards the Trough; the total area of the Guli pluton may thus reach 1600 km<sup>2</sup> (Yegorov, 1991). The pluton is emplaced into a petrographically diverse volcanic package representing different stages of flood basalt magmatism, including melanephelinites of the Arydzhangsky Suite (251.7 ± 0.4 Ma) to the northeast, stratigraphically higher melanephelinites and trachy-rhyodacites of the Del'kansky Suite (251.1 ± 0.3 Ma) to the southwest, and tholeiitic basalts of the Kogotoksky Suite in the east and south (Yegorov, 1991; Kamo *et al.*, 2003). Field observations and geophysical data indicate that contacts between the Guli complex and its host volcanics are nearly vertical (Yeliseev and Sheinman, 1961).

The complex comprises predominantly dunites and melanephelinites, which collectively make up ~90% of the exposed area; the remainder is represented by a wide variety of ultramafic,

alkaline and carbonatitic plutonic and hypabyssal rocks (Yegorov, 1991). On the basis of field evidence, Yegorov (1969, 1991) proposed the following order of their emplacement (oldest to youngest): dunites; magnetite-bearing, perovskite-free clinopyroxenites (koswites); melilitolites (*sensu lato*); melteigite–shonkinite series rocks; melanephelinites and alkali picrites; jacupirangite–melteigite series rocks (characterised by the abundance of perovskite); ijolites; nepheline and alkali-feldspar syenites (locally silica-oversaturated); phoscorites; carbonatites. Our own field and petrographic observations indicate that at least some of the alkali-feldspar syenites are probably fenitised rafts of basement rocks, rather than intrusive units. This interpretation is supported by their low negative  $\epsilon\text{Nd}$  and high initial  $^{87}\text{Sr}/^{86}\text{Sr}$  values (Kogarko and Zartman, 2007). It is also noteworthy that the dunites are viewed by some researchers as much older rocks unrelated to the Permian–Triassic event (Malitch *et al.*, 2011).

Carbonatites form two large stocks, crudely oval in plan view and measuring ca. 5 and 3 km<sup>2</sup> (Southern and Northern, respectively), and numerous dykes emplaced into the alkali-ultramafic units (Fig. 1b). The exposed part of the Northern stock consists almost exclusively of calcite carbonatites, although phoscorites were reported to occur as dykes south of this intrusion and as xenoliths in the carbonatites (Yegorov, 1991). The Southern carbonatite intrusion is more complex, consisting of coarse-grained calcitic rocks along its western, northern and north-eastern margins, and dolomite carbonatites in the southern part which is dissected by the Gule River. The two stocks are separated by a large (~4 × 1–2 km) body of jacupirangites, melteigites and subordinate ijolites. Along its northern contact, the Southern stock is bordered by melilitolites and products of their metasomatic reworking. Field relations suggest that the carbonatites postdate all ultramafic and alkaline silicate rocks, with the exception of thin lamprophyre dykes that were observed locally to crosscut the carbonatites (Yegorov, 1991). The bulk of carbonatite intrusions at Guli are represented by modally simple rocks, composed of 85–95 vol.% carbonate with subordinate magnetite, apatite and phlogopite. However, their endocontact zones adjacent to ultramafic and alkaline wall-rocks or their xenoliths are mineralogically complex and contain a high proportion (locally, up to 60 vol.%) of silicate and oxide phases, including forsterite, diopside, phlogopite, calcic garnets, richterite, magnetite, perovskite, baddeleyite and calzirtite. In particular, the well-exposed contacts of calcite carbonatites with ultramafic rocks in the southern part of the Northern stock and in the western part of the Southern stock contain abundant euhedral perovskite crystals, which are not observed either in the exocontact or further towards the interior of these carbonatite bodies. Along the northern contact of the Southern stock, the wall-rock melilitolites are extensively metasomatised to wollastonite–nepheline–calcite–diopside rocks and glimmerites (Yegorov, 1969; authors' unpublished data). The part of this metasomatic aureole proximal to coarse-grained calcite carbonatites (or, possibly, the endocontact facies of the carbonatite itself) is devoid of perovskite, but contains a high proportion of euhedral phlogopite and andradite.

There is a dearth of reliable geochronological data for the Guli complex, particularly taking into consideration its formidable size and compositional diversity. Dalrymple *et al.* (1995, p. 2079) studied a “poorly located biotite sample ... from one of the carbonatite bodies” using  $^{40}\text{Ar}$ – $^{39}\text{Ar}$  radiometric age determination and obtained a plateau age of 437.7 ± 2.0 Ma, which is clearly in conflict with the much younger age of the surrounding volcanic rocks (~251 Ma). Kogarko and Zartman (2007) used whole-rock U–Pb

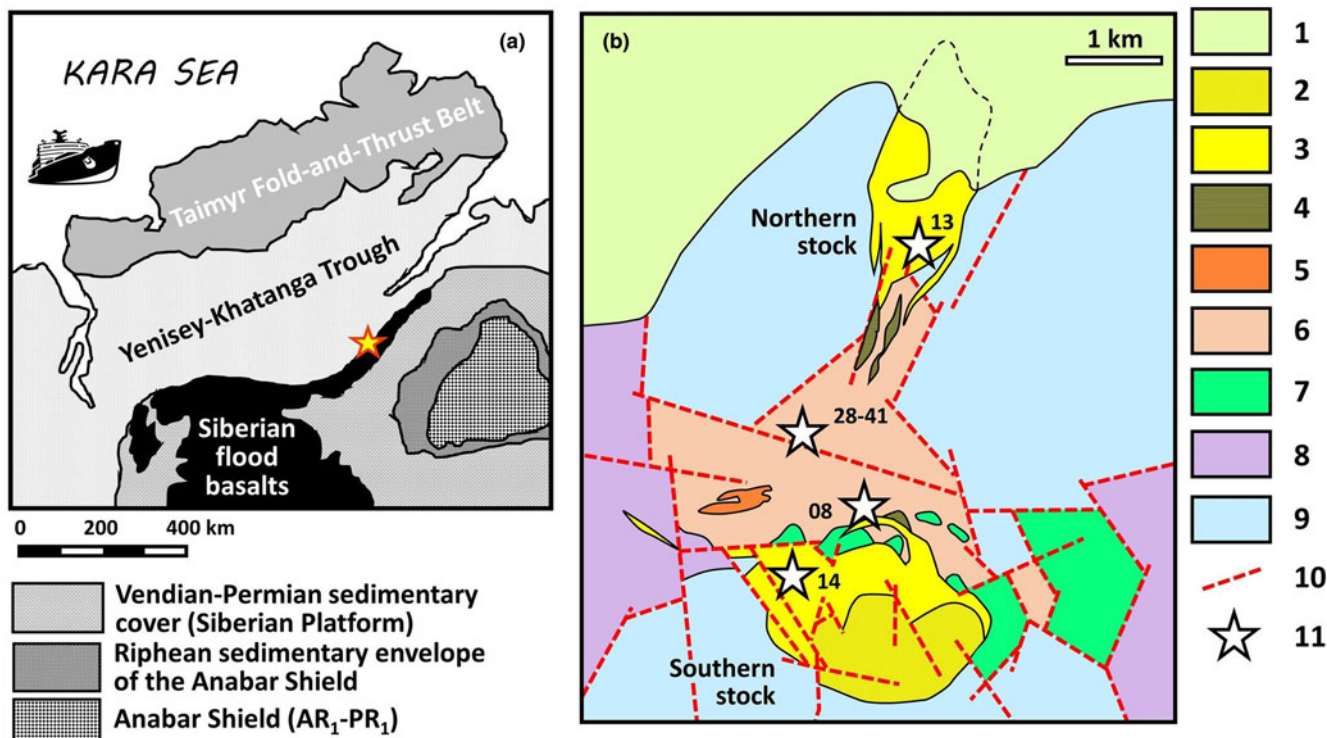


**Fig. 1.** (a) Location map of the Guli complex (indicated by a star) with respect to the principal structural elements of the northern Siberian Platform and Taimyr Peninsula. (b) Schematic geological map of the central part of the Guli alkaline-ultramafic complex (simplified after Yegorov, 1991): (1) Quaternary sediments; (2) dolomite carbonatites; (3) calcite carbonatites (undifferentiated); (4) phoscorites; (5) alkaline syenites; (6) jacupirangite–melteigite series; (7) melilitolites; (8) dunites; (9) melanephelinites; (10) fault zones and (11) sampling locations.

isotopic data for a wide spectrum of rocks (from dunites to carbonatites) to construct a  $^{238}\text{U}$ – $^{206}\text{Pb}$  isochron and arrive at a rough estimate of their emplacement age ( $250 \pm 9$  Ma). Kamo *et al.* (2003) studied a baddeleyite sample from an unspecified carbonatite locality and paragenesis, and reported a discordant  $^{206}\text{Pb}/^{238}\text{U}$  age of  $250.2 \pm 0.3$  Ma. These authors explained the discordance due to excess  $^{207}\text{Pb}$  by isotopic disequilibrium caused by magma fractionation. A similar value ( $250.8 \pm 1.2$  Ma) was determined for another sample of baddeleyite by Malich *et al.* (2015). The same authors reported a U–Th–Pb chemical isochron age of  $250.1 \pm 2.9$  Ma for thorianite. No paragenetic or provenance information were given for either of the minerals. Remarkably, there appears to have been no attempt to examine the geochronology of perovskite, which is a common accessory mineral in most of the rock types, with the exception of dunites, magnetite clinopyroxenes, shonkinites and alkali-feldspar syenites. Moreover, the relative timing of perovskite crystallisation can be readily constrained on the basis of its distribution within the rock (see above) and textural relations with other minerals (in particular, titanite, calcic garnets and magnetite).

## Analytical methods

### Electron-microprobe analysis

For a detailed geochronological study, we selected three samples of perovskite and one sample of andradite. All samples were examined initially using polarising microscopy, back-scattered electron (BSE) imaging and wavelength-dispersive X-ray spectrometry (WDS) to determine the extent of their compositional variation and confirm that they were not affected by alteration. BSE images and WDS data

were acquired with a Cameca SX100 electron-microprobe at the University of Manitoba (Winnipeg, Canada) operated at a beam current of 10 nA and an accelerating voltage of 15 kV. For perovskite analyses, a 1  $\mu\text{m}$  beam and the following calibration standards were employed: albite ( $\text{NaK}\alpha$ ), andalusite ( $\text{AlK}\alpha$ ), diopside ( $\text{CaK}\alpha$ ,  $\text{SiK}\alpha$ ), titanite ( $\text{TiK}\alpha$ ), fayalite ( $\text{FeK}\alpha$ ), zircon ( $\text{ZrL}\alpha$ ), synthetic  $\text{SrTiO}_3$  ( $\text{SrL}\alpha$ ),  $\text{Ba}_2\text{NaNb}_5\text{O}_{15}$  ( $\text{NbL}\alpha$ ), REE orthophosphates ( $\text{LaL}\alpha$ ,  $\text{CeL}\alpha$ ,  $\text{PrL}\beta$ ,  $\text{NdL}\beta$ ) and  $\text{ThO}_2$  ( $\text{ThM}\alpha$ ). Potassium, Ba, Sm, Ta and U were sought, but not detected in any of the samples. The andradite composition was determined using a 10  $\mu\text{m}$  beam and the same standards as above for Na, Al, Ca, Si, Ti, Fe and Nb, plus forsterite ( $\text{MgK}\alpha$ ) and spessartine ( $\text{MnK}\alpha$ ). Fluorine, Zr and REE were also sought, but not detected.

### LA-ICPMS

The LA-ICPMS-based U–Pb geochronological study of perovskite was performed using a 213 nm Nd-YAG laser ablation system (UP-213, Merchantek) attached to a ThermoFinnigan Element 2 sector-field ICPMS at the University of Manitoba (Winnipeg, Canada). Laser ablation was performed *in situ* for two samples from calcite carbonatites (GU-13 and GU-14) using the parameters listed in Table 1. Uranium and Pb concentrations were determined by the LA-ICPMS prior to the U–Th–Pb isotope measurements following the procedure described in Reguir *et al.* (2010).

For the LA-ICPMS U–Pb geochronological study of perovskite, zircon GJ-1 (609 Ma; Jackson *et al.*, 2004) was employed as a primary standard. The quality control was achieved by using the natural Ice River perovskite (Heaman, 2009) as a secondary standard. In order to minimise the number of large particles

**Table 1.** LA-ICPMS operating and data-acquisition parameters.

<b>ICP-MS</b>	
Model	Element 2
Plasma Power	1330 Watt
Gas flows:	
Plasma (Ar)	~14.8 L min <sup>-1</sup>
Auxiliary (Ar)	~1.1 L min <sup>-1</sup>
Sample (Ar/He)	~0.86/0.58 L min <sup>-1</sup>
<b>LA</b>	
Model	New Wave Research UP-213
Beam sizes:	
Calibration standard GJ-1	45×24 μm
Sample	55 μm
Repetition rates:	
Calibration standard GJ-1	2 Hz
Sample	4 Hz
Energy densities:	
Calibration standard GJ-1	~3.55 J cm <sup>-2</sup>
Sample	~4.5 J cm <sup>-2</sup>
<b>Data acquisition parameters</b>	
Sample time	0.01 s
Samples per peak	100
Segment duration	0.5 s
Integration window	5%
Scan method	EScan

entering the plasma and to smooth the noisy signals from the relatively low repetition rates, a dual spray chamber, combining the Scott-type and cyclonic-type chambers, was attached to the plasma torch. All analyses were performed using Ni skimmer and sample cones to minimise Pt oxide interferences on Pb. The instrument was tuned using NIST SRM 610 to maintain oxide formation rates at ~0.1% (ThO/Th) and Th/U ratios at ~0.8 to minimise elemental fractionation at the ion source. Each analysis consisted of a 30 s blank measurement prior to laser ablation. The signal intensities were acquired for 30 s in a time-resolved mode for the following isotopes: <sup>202</sup>Hg, <sup>204</sup>Pb, <sup>204</sup>Hg, <sup>206</sup>Pb, <sup>207</sup>Pb, <sup>208</sup>Pb, <sup>232</sup>Th, <sup>235</sup>U and <sup>238</sup>U. Although <sup>202</sup>Hg and <sup>204</sup>Hg were measured, <sup>204</sup>Pb corrections were not applied because of high errors associated with this procedure (Reguir *et al.*, 2010).

In order to correct for instrumental drift, two measurements of the GJ-1 primary standard were performed for every 5–10 unknowns. In non-matrix-matched U–Pb age determination, it is critical to match the patterns of elemental fractionation between the primary standard and unknowns. To minimise elemental fractionation at the ablation site, GJ-1 zircon was ablated using a beam focused at 300 μm below the surface, resulting in the ellipse-shaped footprint at the surface (Table 1). To reduce the elemental fractionation further, the repetition rate was set to 2 Hz, resulting in ~18 μm deep ablation pits. The ablation depth was measured by focus differences between the surface and bottom of a laser pit under an optical microscope. With the optimised laser conditions, no signs of time-dependant fractionation between U and Pb in GJ-1 were observed. Perovskite measurements were more straightforward and required fewer adjustments (Table 1) because of its ability to absorb laser energy more efficiently than zircon. Potential elemental fractionation at the ion source, caused by incomplete vaporisation of laser aerosols (e.g. Kuhn and Günther, 2003) was assessed by monitoring the Th/U ratios in GJ-1 and perovskite. We observed no evidence of elemental fractionation in our samples or GJ-1 zircon. With the elemental fractionation kept at a minimum at the ablation site and the ion source, the instrument mass-bias can become an important

source of errors, especially in non-matrix-matched U–Pb LA-ICPMS perovskite age determination. In this study, the degree of instrument mass-bias was evaluated by analysing the Ice River perovskite (Heaman, 2009) as an unknown simultaneously with the Guli samples using GJ-1 as a primary standard.

### ID-TIMS

Geochronological studies of perovskite using ID-TIMS-based U–Pb from carbonatite sample GU-13 and jacupirangite GU-28-41, as well as of andradite from metasomatised melilitolite (GU-08) were undertaken at the Isotope Geology Laboratory of the Institute of Precambrian Geology and Geochronology (IPGG RAS, St. Petersburg, Russia). For this study, visually homogeneous fragments (<0.15 mm) of perovskite and andradite were used. The selected grain fractions were subjected to preliminary ultrasonic cleaning with 1 N HCl (for perovskite) or water (for andradite) followed by acid treatment (6 N HCl or 1 N to 3 N HNO<sub>3</sub> at 80°C for 15–30 min) (DeWolf *et al.*, 1996). The samples were then washed in warm water for 20 min, transferred to a pressure vessel for digestion (Krogh, 1973), spiked with a <sup>202</sup>Pb–<sup>235</sup>U tracer, and dissolved in 0.2 ml of 10:1 mixture of 29 N HF and 15 N HNO<sub>3</sub> at 180–200°C for 24 hours. Lead and U were separated using a novel single-stage technique, which involves the removal of interfering elements (Ca, Fe, etc.) with 3.1 N HCl + 0.5 N HBr prior to the separation of Pb and U with 6 N HCl and H<sub>2</sub>O, respectively (Corfu and Andersen, 2002). In some cases, U was purified with UTEVA resin (Horwitz *et al.*, 1992). The uncertainties of the measured U/Pb ratios, U and Pb concentrations were 0.5%, and the blanks were 10 pg for Pb and 1 pg for U.

Isotopic ratios were measured using a Triton TI multi-collector mass-spectrometer equipped with a Daly detector in digital ion-counting mode. A thermal mass-fractionation correction of 0.1%/amu for Pb and U was derived by replicate analyses of the SRM 981 and SRM 982 NBS standards. The uncertainties of the measured Pb and U concentrations and U/Pb ratios were 0.5%. The errors were calculated by propagating the within-run error for measured isotopic ratios, the uncertainty in fractionation (±0.03% for Pb and U amu), the uncertainty in Pb and U blank concentration (±50%), the uncertainty in spike calibration (±0.5%), ±0.1 absolute uncertainty in Pb blank composition, and external reproducibility of the 91500 zircon standard (Wiedenbeck *et al.*, 2002). Procedural blanks were ~10 pg for Pb and ~1 pg for U. The data were reduced using the *PbDAT* (Ludwig, 1991) and *ISOPLLOT* (Ludwig, 2003) software. Correction for common Pb was applied according to the model of Stacey and Kramers (1975), all errors are reported here as 2σ.

### Research material: provenance and compositional variations

Drill-core sample GU-28-41 (70°54'39"N, 101°14'07"E) is a melanocratic, coarse-grained rock, sampled from a depth of 41 m in the jacupirangite–melteigite intrusion separating the two carbonatite stocks (Fig. 1b). The rock comprises prismatic crystals of diopside locally replaced by phlogopite, and relatively abundant (~4–8 vol.%) euhedral, zoned crystals of perovskite up to 3 mm across (Fig. 2a). Although this sample should be termed clinopyroxenite on the basis of its modal composition (Le Maitre, 2002), we will retain the name 'jacupirangite' used in the previous literature to distinguish it from perovskite-free rocks of the first intrusive phase (Yegorov, 1991; Kogarko *et al.*, 2007). According to

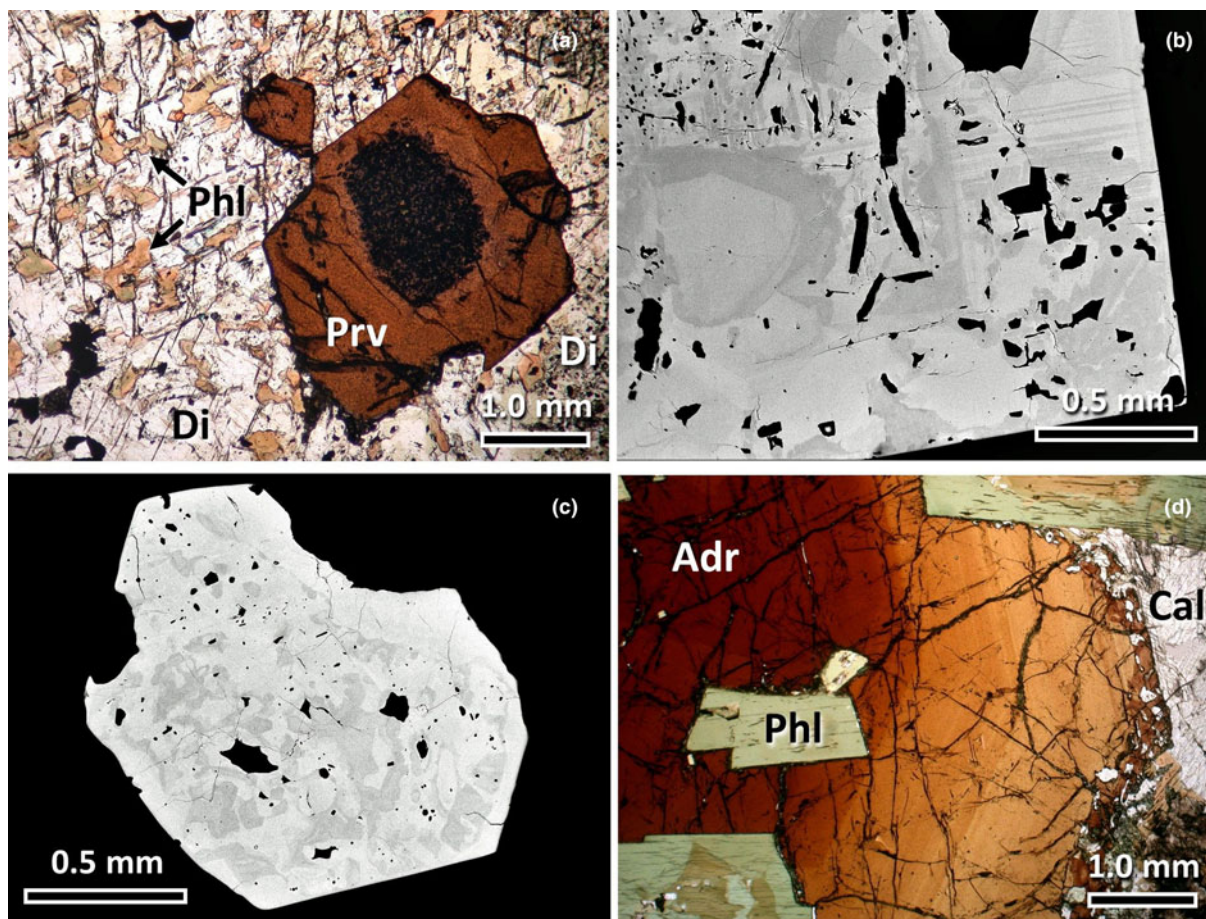


**Fig. 2.** (a) Plane-polarised light (PPL) image of perovskite (Prv) associated with diopside (Di) and phlogopite (Phl) in jacupirangite; sample GU-28-41. (b) Back-scattered electron (BSE) image of cubic perovskite crystal from the Northern carbonatite stock, sample GU-13. (c) BSE image of cuboctahedral perovskite crystal from the Southern carbonatite stock, sample GU-14. (d) PPL image of zoned andradite (Adr) at the contact of calcite carbonatite (Cal) with metasedimented melilitolite, sample GU-08.

Yegorov (1991), this sample represents Subphase 3 of the third intrusive phase (jacupirangite–melteigite series). Perovskite crystals have a turbid, purplish-brown, inclusion-rich core and a clear brown rim. The core is enriched in Al, Fe, Nb and REE relative to the rim, which shows elevated concentrations of Na and Zr (Fig. 3a–c; Table 2). The ovoid inclusions in perovskite cores contain diopside, phlogopite, apatite, magnetite, pectolite and an unidentified Na-K-bearing silicate material.

Sample GU-13 (Lat. 70°55'19"N, Long. 101°17'00"E) was collected from the southernmost exposure of coarse-grained phlogopite-apatite-magnetite-perovskite-rich calcite carbonatite near the intrusive contact between the Northern stock and its ultramafic wall-rocks. Perovskite in this sample forms lustrous cubic crystals up to 5 mm across. In BSE images, the crystals reveal abundant inclusions of apatite and a complex zoning pattern comprising a small anhedral core and multiple oscillatory growth zones (Fig. 2b) characterised by concomitant variation in Na, Fe and Nb at similar levels of Al, Zr and REE (Fig. 3; Table 2).

Sample GU-14 (70°53'00"N, 101°14'15"E) is a coarse-grained calcite carbonatite collected from near the western contact of the Southern stock with clinopyroxenites. The carbonatite contains cuboctahedral crystals up to 1 cm in size associated with diopside and phlogopite. The crystals exhibit patchy zoning in BSE images (Fig. 2c) arising from higher levels of Fe and Nb in brighter areas (Fig. 3).

Garnet GU-08 (70°53'35"N, 101°15'50"E) was collected from the contact zone between calcite carbonatite of the Southern stock and wollastonite-calcite-nepheline-diopside metasomatic rocks developed at the expense of melilitolites. This sample is essentially a bi-mineralic, coarse-grained aggregate of euhedral green phlogopite and subhedral black andradite crystals up to several cm in size. Platy zoned crystals of phlogopite are enclosed in the garnet or encrust the contact between the metasedimented melilitolite and calcite. Andradite crystals of dodecahedral–trapezohedral habit are invariably euhedral with respect to calcite, but anhedral with respect to the metasomatic endocontact. In plane-polarised light, the andradite exhibits concentric zoning comprising a dark reddish-brown core, sandy- to pale-brown intermediate zone and a dark-brown, poikilitic rim (Fig. 2d). The core has higher concentrations of Mg and Ti, but lower levels of Al and Fe relative to the intermediate zone. The rim is further depleted in Mg and enriched in Fe, but contains lower Al in comparison with the intermediate zone (Fig. 3d; Table 3).

## Data reduction and age determination

### LA-ICPMS U–Pb geochronology

The concentrations of U in the perovskite investigated vary from 170 ppm in the samples from carbonatites to 35 ppm in that from

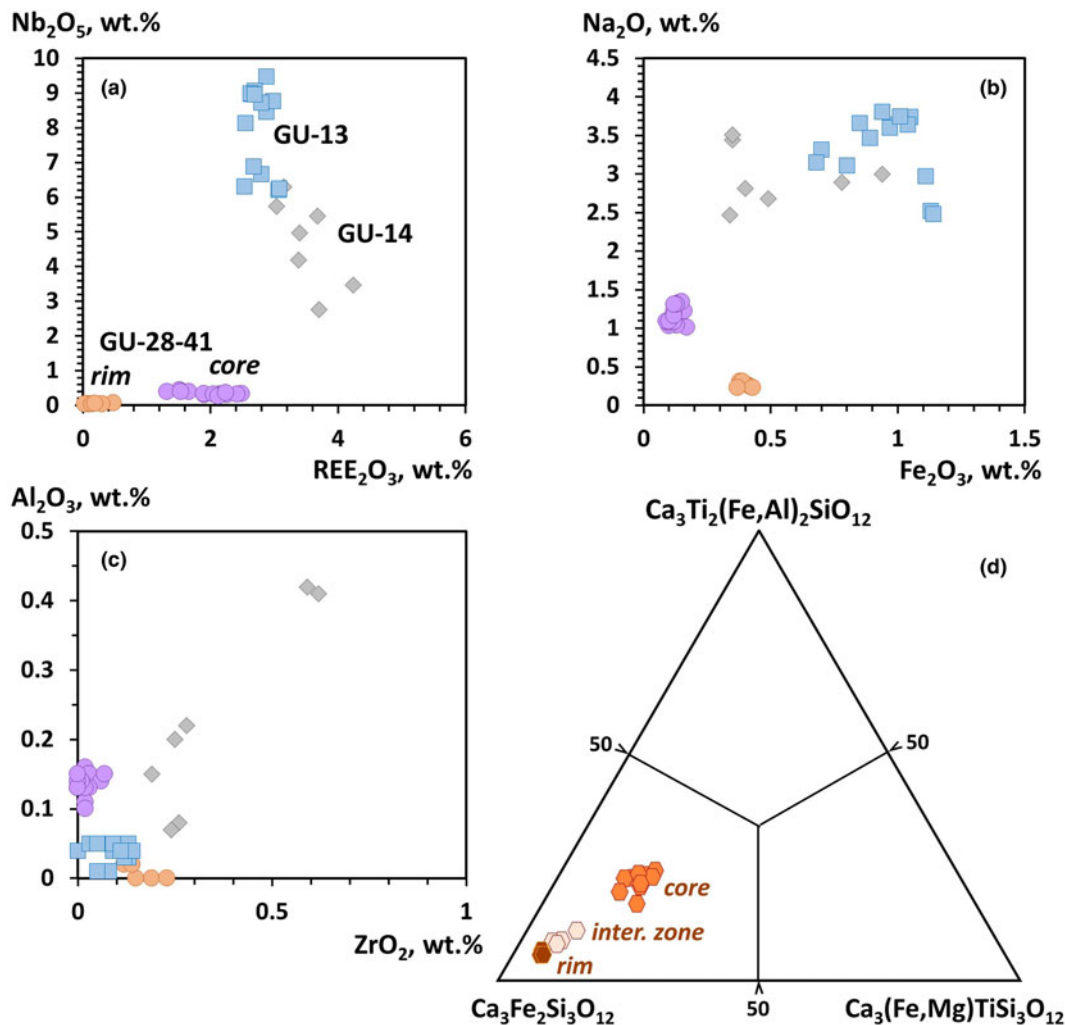


**Fig. 3.** Compositional variation of perovskite (a–c) and andradite (d) samples studied in the present work. (a–c) Variations in the contents of major and minor elements (wt.% oxides) in zoned perovskite crystals from jacupirangite (GU-28-41: circles) and calcite carbonatites (GU-13: squares, GU-14: diamonds). (d) Variation in the proportion of major end-member components in zoned andradite from the contact of calcite carbonatite with metasomatised melilite (GU-08).

jacupirangite. The data reduction for U–Pb age determination of perovskite using LA-ICPMS was performed using the *VisualAge DRS* procedure (Petrus and Kamber, 2012) in the *Iolite 3.7* software (Paton *et al.*, 2011). Following the calculation procedure used to determine the U–Pb age of perovskite from the Afrikanda complex, Kola (Reguir *et al.*, 2010), the isotopic composition of common Pb in perovskite from Guli was calculated using the Stacey and Kramers (1975) two-stage growth model for the inferred age of the sample. This technique is conventionally employed in U–Pb isotopic studies of geological materials of various provenance and age (e.g. Frei and Gerdes, 2009; Tappe and Simonetti, 2012; Castillo-Oliver *et al.*, 2016). The common lead corrected  $^{206}\text{Pb}/^{238}\text{U}$  ratios and ages of each individual perovskite analysis (Table 4) were calculated using *Isoplot/Ex 3.75* (Ludwig, 2012) applying the following decay constants:  $9.8485 \times 10^{-10} \text{ a}^{-1}$  for  $^{235}\text{U}$  and  $1.55125 \times 10^{-10} \text{ a}^{-1}$  for  $^{238}\text{U}$  (Steiger and Jäger, 1977). The uncertainties in determination of common Pb isotopic compositions were numerically propagated through the error calculations by *Isoplot/Ex 3.75* (Ludwig, 2012). The weighted mean of 30 analyses of perovskite from sample GU-13 yielded a  $^{206}\text{Pb}/^{238}\text{U}$  age of  $250.4 \pm 1.1 \text{ Ma}$  (Fig. 4a). The age of perovskite from sample GU-14, obtained by taking the

weighted mean of 30 analyses, corresponds to  $255.3 \pm 2.4 \text{ Ma}$  (Fig. 4b). *Isoplot/Ex 3.75* was also used to construct the Tera–Wasserburg diagram (Tera and Wasserburg, 1972), which yielded  $^{206}\text{Pb}/^{238}\text{U}$  ages of  $249.3 \pm 4.7 \text{ Ma}$  and  $254.6 \pm 3.7 \text{ Ma}$  for GU-13 and GU-14, respectively. The Tera–Wasserburg diagram was constructed by anchoring the data at a selected  $^{207}\text{Pb}/^{206}\text{Pb}$  ratio applying the common Pb composition determined using the Stacey and Kramers (1975) model.

The U–Pb data for the Ice River material acquired using the GJ-1 zircon calibration standard and the same procedure as that applied to the Guli perovskite (Table 5) yielded a weighted average age of  $357.2 \pm 2.4 \text{ Ma}$  (Fig. 6). This result is within the analytical uncertainty from the value of  $356.5 \pm 1 \text{ Ma}$  recommended by Heaman (2009) and is close to the 360–364 Ma range reported by Tappe and Simonetti (2012).

#### ID-TIMS U–Pb geochronology

The U–Pb ID-TIMS data were reduced using the *PbDAT* (Ludwig, 1991) and *Isoplot* (Ludwig, 2003) software. The results are reported in Table 6, with all uncertainties quoted as  $2\sigma$ . The common Pb corrections for ID-TIMS analyses were performed using

**Table 2.** Representative WDS compositions (wt.% oxide) and formulae (apfu) of perovskite from Guli.

Oxides	GU-28-41			GU-14	GU-13
	core	rim	outer rim		
Wt.%					
Na <sub>2</sub> O	0.12	0.13	0.43	0.34	0.68
CaO	39.76	39.27	40.2	37.65	37.55
SrO	0.24	0.16	0.45	0.20	0.26
La <sub>2</sub> O <sub>3</sub>	0.37	0.34	n.d.	0.90	0.75
Ce <sub>2</sub> O <sub>3</sub>	0.81	1.25	n.d.	1.84	1.17
Pr <sub>2</sub> O <sub>3</sub>	n.d.	n.d.	n.d.	0.28	0.17
Nd <sub>2</sub> O <sub>3</sub>	0.36	0.44	n.d.	0.68	0.44
Sm <sub>2</sub> O <sub>3</sub>	n.d.	n.d.	n.d.	0.16	n.d.
Al <sub>2</sub> O <sub>3</sub>	0.14	0.15	n.d.	0.20	0.05
Fe <sub>2</sub> O <sub>3</sub>	1.08	1.31	0.23	2.47	3.15
TiO <sub>2</sub>	56.44	55.73	58.52	52.22	50.44
ZrO <sub>2</sub>	n.d.	n.d.	0.15	0.25	n.d.
Nb <sub>2</sub> O <sub>5</sub>	0.39	0.25	n.d.	2.76	6.31
Ta <sub>2</sub> O <sub>5</sub>	n.d.	n.d.	n.d.	n.d.	n.d.
Total	99.55	99.71*	99.14	99.95	100.97
Atoms per formula unit (apfu) calculated to three atoms of oxygen					
Na	0.005	0.006	0.019	0.015	0.031
Ca	0.979	0.976	0.978	0.946	0.935
Sr	0.003	0.002	0.006	0.003	0.004
La	0.003	0.003	-	0.008	0.006
Ce	0.007	0.011	-	0.016	0.010
Pr	-	-	-	0.002	0.001
Nd	0.003	0.004	-	0.006	0.004
Sm	-	-	-	0.001	-
ΣA cations	1.000	1.003*	1.003	0.997	0.991
Al	0.004	0.004	-	0.006	0.001
Fe <sup>3+</sup>	0.019	0.023	0.004	0.044	0.055
Ti	0.976	0.972	0.999	0.921	0.882
Zr	-	-	0.002	0.003	-
Nb	0.004	0.003	-	0.029	0.066
Ta	-	-	-	-	-
ΣB cations	1.003	1.002	1.005	1.003	1.004

n.d. = not detected. \*Total includes 0.11 wt.% ThO<sub>2</sub> (0.001 apfu Th).

two approaches, the two-stage Pb evolution model of Stacey and Kramers (1975) and three-dimensional linear isochron (Ludwig, 2003). The latter technique allows the assessment of data concordance and of the assumption of invariant common Pb composition. The concordia-constrained three-dimensional linear isochron age determined for the four perovskite fractions is  $253 \pm 2$  Ma (MSWD = 2.0), which is in excellent agreement with the concordia age obtained using the Stacey and Kramers (1975) model ( $250 \pm 1$  Ma for GU-28-41 and  $249 \pm 2$  Ma for GU-13; Fig. 7). The initial common Pb composition, derived from this isochron ( $^{206}\text{Pb}/^{204}\text{Pb} = 17.5 \pm 4.3$  and  $^{207}\text{Pb}/^{204}\text{Pb} = 15.49 \pm 0.24$ ) corresponds to the concordia  $^{206}\text{Pb}/^{238}\text{U}$  ages of  $253 \pm 2$  Ma (MSWD = 0.65) for GU-28-41 and  $252 \pm 1$  Ma (MSWD = 1.3) for GU-13. The andradite sample (GU-08) is characterised by much lower U levels ( $\sim 4\text{--}7$  ppm) compared to perovskite, and gave slightly discordant results, with an average  $^{206}\text{Pb}/^{238}\text{U}$  age of  $247 \pm 6$  Ma (Fig. 7).

## Discussion and conclusions

The timing of alkaline and carbonatitic magmatism in the Maimecha–Kotuy Province and Taimyr Peninsula and its connection to the Siberian flood basalts at the Permian–Triassic boundary has been addressed at length in previous studies (e.g. Dalrymple *et al.*, 1995; Vernikovskiy *et al.*, 2003; Ivanov, 2013; Burgess and Bowring, 2015; Reichow *et al.*, 2016). The voluminous geochronological literature on the Siberian basaltic volcanism

**Table 3.** Representative WDS compositions (wt.% oxide) and formulae (apfu) of andradite from Guli.

	1	2	3
Wt.% oxide			
Na <sub>2</sub> O	0.10	n.d.	0.04
MgO	0.90	0.46	0.29
CaO	33.22	33.75	33.47
MnO	0.26	0.13	0.20
FeO	0.20	n.d.	0.32
Al <sub>2</sub> O <sub>3</sub>	1.52	2.19	1.06
Fe <sub>2</sub> O <sub>3</sub>	24.17	26.22	28.15
SiO <sub>2</sub>	30.53	33.98	34.76
TiO <sub>2</sub>	9.55	3.88	2.83
Total	100.45	100.61	101.12
Atoms per formula unit calculated to eight cations and 12 oxygens			
Na	0.016	-	0.006
Mg	0.113	0.057	0.036
Ca	2.991	3.009	2.985
Mn	0.019	0.009	0.014
Fe <sup>2+</sup>	0.014	-	0.022
Al	0.151	0.215	0.104
Fe <sup>3+</sup>	1.528	1.642	1.763
Si	2.565	2.827	2.893
Ti	0.603	0.243	0.177

n.d. = not detected

has not reached a consensus with regard to the duration or spatial extent of this event. High-precision geochronology of zircon from gabbroic intrusions and pyroclastic deposits in the peripheral

**Table 4.** LA-ICPMS U–Pb results for perovskite from the Guli carbonatites.

Analysis No.	Measured ratios				Fraction of common lead		Corrected ratios		Apparent ages	
	$^{207}\text{Pb}/^{206}\text{Pb}$	$\pm 2\sigma$	$^{238}\text{U}/^{206}\text{Pb}$	$\pm 2\sigma$	$f$	$\pm 2\sigma$	$^{206}\text{Pb}/^{238}\text{U}$	$\pm 2\sigma$	Ma	$\pm 2\sigma$
<b>GU-13</b>										
1	0.2530	0.0110	18.7970	0.6360	0.2519	0.0137	0.0398	0.0015	251.6	9.5
2	0.2540	0.0120	18.7970	0.7420	0.2532	0.0150	0.0397	0.0018	251.2	10.9
3	0.2480	0.0130	18.2482	0.7326	0.2452	0.0162	0.0414	0.0019	261.3	11.7
4	0.2620	0.0130	18.8324	0.6384	0.2633	0.0162	0.0391	0.0016	247.4	9.8
5	0.2620	0.0110	18.6916	0.5939	0.2632	0.0137	0.0394	0.0015	249.2	9.0
6	0.2610	0.0110	17.7620	0.5679	0.2614	0.0137	0.0416	0.0015	262.6	9.5
7	0.2176	0.0084	19.8020	0.6666	0.2076	0.0105	0.0400	0.0014	252.9	9.0
8	0.2390	0.0100	19.8807	0.6324	0.2347	0.0125	0.0385	0.0014	243.5	8.5
9	0.2410	0.0110	19.1939	0.6263	0.2369	0.0137	0.0398	0.0015	251.3	9.2
10	0.2480	0.0120	18.9036	0.5718	0.2456	0.0150	0.0399	0.0014	252.3	9.0
11	0.2610	0.0120	18.5874	0.6219	0.2619	0.0150	0.0397	0.0016	251.0	9.6
12	0.2128	0.0085	19.4932	0.6080	0.2014	0.0106	0.0410	0.0014	258.8	8.6
13	0.2590	0.0130	19.7239	0.6614	0.2600	0.0162	0.0375	0.0015	237.4	9.3
14	0.2390	0.0100	18.9394	0.5739	0.2342	0.0125	0.0404	0.0014	255.5	8.6
15	0.2640	0.0110	18.7617	0.6688	0.2658	0.0137	0.0391	0.0016	247.5	9.8
16	0.2310	0.0100	19.6078	0.6920	0.2245	0.0125	0.0396	0.0015	250.1	9.5
17	0.2130	0.0110	20.3666	0.7052	0.2021	0.0137	0.0392	0.0015	247.7	9.4
18	0.2180	0.0100	20.5339	0.7168	0.2085	0.0125	0.0385	0.0015	243.8	9.2
19	0.2430	0.0100	19.1939	0.5894	0.2394	0.0125	0.0396	0.0014	250.5	8.6
20	0.2270	0.0100	20.2840	0.5349	0.2198	0.0125	0.0385	0.0012	243.3	7.4
21	0.2243	0.0095	18.8679	0.7120	0.2156	0.0119	0.0416	0.0017	262.6	10.5
22	0.2360	0.0110	20.1613	0.6504	0.2311	0.0137	0.0381	0.0014	241.3	8.7
23	0.2000	0.0110	21.5517	0.8825	0.1862	0.0137	0.0378	0.0017	238.9	10.4
24	0.2080	0.0110	19.1205	0.7677	0.1952	0.0137	0.0421	0.0018	265.8	11.4
25	0.1894	0.0096	20.6612	0.7684	0.1724	0.0120	0.0401	0.0016	253.2	9.9
26	0.3160	0.0180	16.8919	0.6848	0.3306	0.0225	0.0396	0.0021	250.5	12.9
27	0.2820	0.0140	18.3150	0.6373	0.2884	0.0175	0.0389	0.0017	245.7	10.3
28	0.3400	0.0140	16.2338	0.5534	0.3606	0.0175	0.0394	0.0017	249.0	10.7
29	0.1970	0.0095	20.6612	0.6830	0.1820	0.0119	0.0396	0.0014	250.3	8.9
30	0.2036	0.0099	20.7039	0.7287	0.1904	0.0124	0.0391	0.0015	247.3	9.3
<b>GU-14</b>										
1	0.1917	0.0081	19.8413	0.6692	0.1749	0.0101	0.0416	0.0015	262.6	9.2
2	0.1503	0.0078	21.6920	0.7058	0.1235	0.0097	0.0404	0.0014	255.3	8.6
3	0.1644	0.0084	21.5054	0.8325	0.1412	0.0105	0.0399	0.0016	252.4	10.0
4	0.2090	0.0110	19.4932	0.6840	0.1966	0.0137	0.0412	0.0016	260.4	10.0
5	0.1657	0.0078	20.7039	0.6858	0.1425	0.0097	0.0414	0.0015	261.6	9.0
6	0.1685	0.0080	21.6450	0.8433	0.1465	0.0100	0.0394	0.0016	249.3	9.9
7	0.1827	0.0085	20.4499	0.7109	0.1639	0.0106	0.0409	0.0015	258.3	9.4
8	0.1522	0.0080	22.4215	0.8044	0.1262	0.0100	0.0390	0.0015	246.4	9.1
9	0.1764	0.0087	20.9644	0.7472	0.1562	0.0109	0.0403	0.0015	254.4	9.5
10	0.1677	0.0086	21.3675	0.7762	0.1454	0.0107	0.0400	0.0015	252.8	9.5
11	0.1847	0.0090	20.5761	0.6351	0.1665	0.0112	0.0405	0.0014	256.0	8.5
12	0.1729	0.0096	21.4592	0.7828	0.1520	0.0120	0.0395	0.0015	249.9	9.6
13	0.1583	0.0079	21.5054	0.7862	0.1336	0.0099	0.0403	0.0015	254.6	9.6
14	0.2210	0.0110	20.1207	0.7287	0.2121	0.0137	0.0392	0.0016	247.6	9.8
15	0.1809	0.0096	19.6464	0.7334	0.1612	0.0120	0.0427	0.0017	269.5	10.5
16	0.2160	0.0110	19.8413	0.7874	0.2056	0.0137	0.0400	0.0017	253.1	10.7
17	0.1840	0.0100	20.6612	0.7257	0.1656	0.0125	0.0404	0.0015	255.2	9.6
18	0.1696	0.0090	21.4592	0.7368	0.1478	0.0112	0.0397	0.0015	251.1	9.1
19	0.1573	0.0086	21.1864	0.8080	0.1322	0.0107	0.0410	0.0016	258.8	10.2
20	0.4370	0.0170	13.5135	0.5296	0.4821	0.0212	0.0383	0.0022	242.4	13.5
21	0.2090	0.0100	20.2020	0.7754	0.1970	0.0125	0.0398	0.0016	251.3	10.2
22	0.2450	0.0120	18.1488	0.7576	0.2414	0.0150	0.0418	0.0019	264.0	11.9
23	0.1850	0.0100	20.4082	0.7080	0.1668	0.0125	0.0408	0.0015	258.0	9.6
24	0.2180	0.0110	19.3798	0.7136	0.2079	0.0137	0.0409	0.0017	258.2	10.3
25	0.1547	0.0091	21.5517	1.0683	0.1290	0.0114	0.0404	0.0021	255.4	12.8
26	0.1960	0.0110	20.1613	0.8130	0.1805	0.0137	0.0406	0.0018	256.8	11.0
27	0.1710	0.0110	19.7239	0.7781	0.1488	0.0137	0.0432	0.0018	272.4	11.4
28	0.2320	0.0110	19.0840	0.7648	0.2255	0.0137	0.0406	0.0018	256.5	11.0
29	0.2230	0.0120	19.2678	0.7796	0.2142	0.0150	0.0408	0.0018	257.7	11.3
30	0.2030	0.0110	20.2020	0.7754	0.1894	0.0137	0.0401	0.0017	253.6	10.4

areas of the Siberian flood basalts ( $251.35 \pm 0.09$ – $251.90 \pm 0.06$  Ma) indicates that the bulk of basic magma was erupted or emplaced within a narrow time interval ( $\sim 300$  ka) near the

end-Permian mass extinction, but the activity continued for another 500 Ka after the event (Burgess and Bowring, 2015). The ages of perovskite from melanophelinite flows near the base



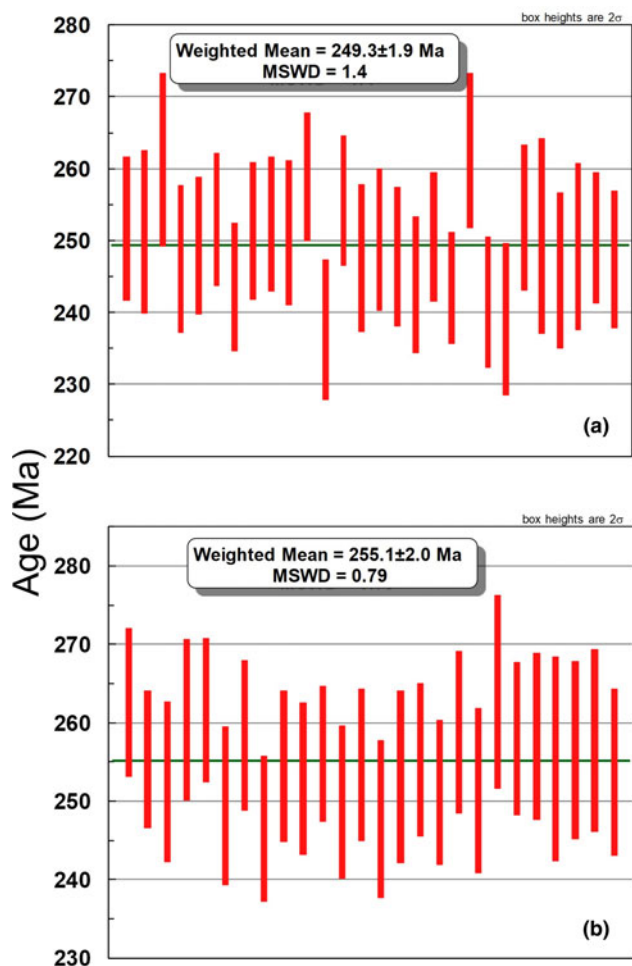


Fig. 4. Weighted mean <sup>206</sup>Pb/<sup>238</sup>U age diagrams for perovskite from the (a) Northern carbonatite stock and (b) Southern stock.

of the basaltic sequence (252.2–252.3 ± 0.1 Ma) provide a robust constraint on the onset of volcanic activity in the Late Permian (Fig. 8 and references therein). Evidence from differentiated alkaline intrusions in the southern margin of the Taimyr Fold-and-Thrust Belt (i.e. across the Yenisey–Khatanga Trough from Guli) suggests that magmatism extended to at least 250.6 ± 0.2 Ma (Augland *et al.*, 2019). The <sup>40</sup>Ar–<sup>39</sup>Ar data for low-Ti tholeiitic flows and their intrusive equivalents from the interior of the Siberian flood basalt province show evidence for a second magmatic pulse some 10 Ma after the extinction, between 242.8 ± 1.3 and 239.1 ± 1.1 Ma (Ivanov *et al.*, 2013). Small-volume mantle magmatism extended even further into the Triassic, as indicated by the recently discovered Carnian (234.0–235.2 Ma) diopside-sanidine-phlogopite lamproites at Norilsk (Ivanov *et al.*, 2018).

The previously published geochronological data for Guli are predominantly limited to carbonatites. Baddeleyite from unknown sampling sites (most likely at the southern contact of the Northern stock) yielded essentially identical ID-TIMS and LA-ICPMS ages: 250.2 ± 0.3 and 250.8 ± 1.2 Ma, respectively (Kamo *et al.*, 2003; Malich *et al.*, 2015). These values are in excellent agreement with our LA-ICPMS data for perovskite from the Northern stock (250.4 ± 1.1 Ma), and are within error from the ID-TIMS results (249 ± 2 Ma) and U–Th–Pb chemical isochron age of thorianite (250.1 ± 2.9 Ma; Malich *et al.*, 2015). Thus, the emplacement of the Northern carbonatite stock is well-constrained and occurred in the waning stage of the first magmatic pulse (Augland *et al.*, 2019). Interestingly, jacupirangites that border the Northern stock from the south (Fig. 1b) are coeval within the analytical uncertainty (250 ± 1 Ma, ID-TIMS).

The LA-ICPMS results for perovskite from the Southern carbonatite stock imply a somewhat older age: its weighted mean <sup>206</sup>Pb/<sup>238</sup>U date is 255.3 ± 2.4 Ma and ‘Tera–Wasserburg’ value 254.6 ± 3.7 Ma (Figs 4, 5). Unfortunately, our attempt to constrain further the age of the Southern stock using andradite from its

Table 5. LA-ICPMS U–Pb results for perovskite from Ice River.

Analysis No.	Measured ratios		Fraction of common lead		Corrected ratios		Apparent ages			
	<sup>207</sup> Pb/ <sup>206</sup> Pb	±2σ	<sup>238</sup> U/ <sup>206</sup> Pb	±2σ	f	±2σ	<sup>206</sup> Pb/ <sup>238</sup> U	±2σ	Ma	±2σ
1	0.1225	0.0086	16.5017	0.5174	0.0857	0.0107	0.0554	0.0019	347.6	11.3
2	0.1150	0.0066	15.8983	0.4550	0.0759	0.0082	0.0581	0.0017	364.2	10.6
3	0.1117	0.0072	16.5563	0.4934	0.0722	0.0089	0.0560	0.0018	351.5	10.7
4	0.1161	0.0074	16.2866	0.4775	0.0775	0.0092	0.0566	0.0018	355.2	10.7
5	0.1090	0.0100	16.7224	0.6152	0.0689	0.0124	0.0557	0.0022	349.3	13.3
6	0.1186	0.0097	16.2866	0.5836	0.0807	0.0120	0.0564	0.0022	354.0	13.1
7	0.1158	0.0074	16.3399	0.4806	0.0772	0.0092	0.0565	0.0018	354.2	10.7
8	0.1042	0.0067	16.2602	0.5288	0.0626	0.0083	0.0577	0.0019	361.3	11.8
9	0.1057	0.0075	16.2866	0.5836	0.0645	0.0093	0.0574	0.0021	360.0	13.0
10	0.1054	0.0061	16.6389	0.5537	0.0643	0.0076	0.0562	0.0019	352.7	11.8
11	0.0964	0.0063	16.8919	0.5992	0.0532	0.0078	0.0561	0.0020	351.6	12.5
12	0.0994	0.0071	16.5017	0.6263	0.0567	0.0088	0.0572	0.0022	358.4	13.6
13	0.1223	0.0083	15.9490	0.5087	0.0851	0.0103	0.0574	0.0019	359.6	11.8
14	0.1101	0.0061	15.6986	0.4929	0.0696	0.0076	0.0593	0.0019	371.2	11.7
15	0.1063	0.0068	16.8067	0.4519	0.0656	0.0084	0.0556	0.0016	348.8	9.6
16	0.1163	0.0086	15.6740	0.6142	0.0773	0.0107	0.0589	0.0024	368.7	14.6
17	0.1298	0.0084	15.5763	0.5580	0.0942	0.0104	0.0582	0.0022	364.4	13.3
18	0.1281	0.0075	15.9744	0.4848	0.0924	0.0093	0.0568	0.0018	356.2	11.1
19	0.1378	0.0066	15.5280	0.4581	0.1042	0.0082	0.0577	0.0018	361.5	10.9
20	0.1166	0.0070	16.2602	0.5288	0.0781	0.0087	0.0567	0.0019	355.5	11.7
21	0.1370	0.0079	15.5521	0.4837	0.1033	0.0098	0.0577	0.0019	361.4	11.6
22	0.0998	0.0058	16.5838	0.4675	0.0573	0.0072	0.0568	0.0017	356.4	10.1
23	0.1038	0.0070	16.4204	0.4853	0.0622	0.0087	0.0571	0.0018	358.0	10.8

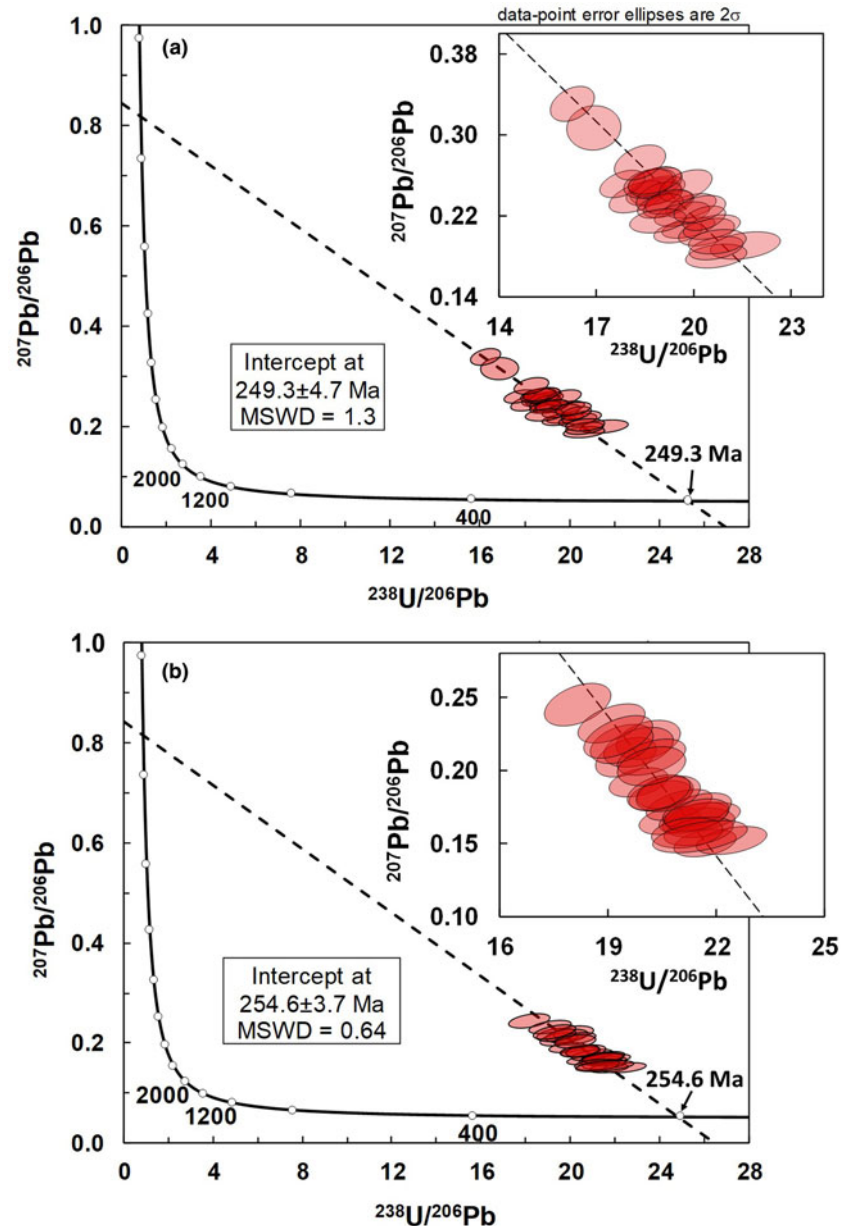


Fig. 5.  $^{207}\text{Pb}/^{206}\text{Pb}$  vs.  $^{238}\text{U}/^{206}\text{Pb}$  diagrams (Tera and Wasserburg, 1972) for perovskite from the (a) Northern carbonatite stock and (b) Southern stock.

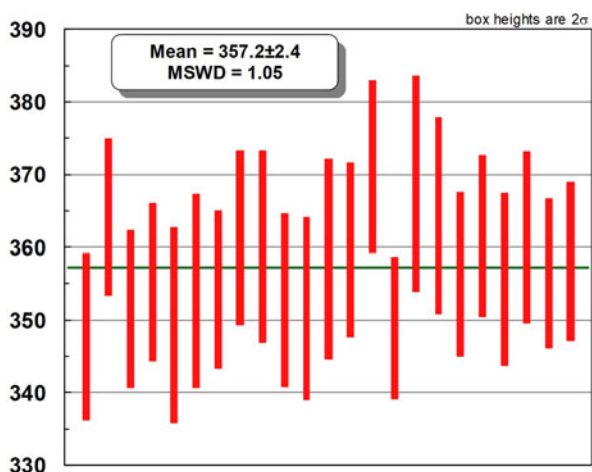


Fig. 6. Weighted mean  $^{206}\text{Pb}/^{238}\text{U}$  age diagrams for perovskite from the Ice River ijolite.

metasomatised contact with melilitolites (GU-08) gave inconclusive results ( $247 \pm 6$  Ma, Fig. 6). Our results are in conflict with the younger U–Pb ages of volcanic rocks outside the Guli complex (Kamo *et al.*, 2003). Notably, however, contacts between the aged-dated Arydzhangsky and Del’kansky Suites and the intrusion are not exposed. Outside these volcanic units, intrusive contacts between the Guli dunites and basalts have been characterised as metasomatic (e.g. Yegorov, 1991, p. 30). However, this interpretation is inconsistent with the much older age of dunites reported by Malich *et al.* (2011), who interpreted these rocks as ophiolite-type blocks of Ediacaran age juxtaposed by alkaline–ultramafic magmas.

The  $\sim 255$  Ma age determined in the present work is not the only indication of pre-Siberian flood basalt magmatism in this part of Siberia. Combined U–Pb data for perovskite from olivinites and phoscorites of the Kugda alkaline–ultramafic complex, situated some 80 km ESE of Guli, gave a value of  $257 \pm 6$  Ma (Anosova *et al.*, 2019), although more precise age determinations for this and other intrusions in the Maimecha–Kotuy province are

**Table 6.** U–Pb ID-TIMS isotopic data<sup>a</sup> for perovskite and andradite from the Guli complex.

No.	Treatment type	Weight (mg)	Pb (ppm)	U (ppm)	Pb <sub>c</sub> /Pb <sub>Σ</sub>	<sup>206</sup> Pb/ <sup>204</sup> Pb <sup>b</sup>	Isotopic ratios corrected for blank and common Pb					Rho <sup>c</sup>	Age (Ma)		
							<sup>208</sup> Pb/ <sup>206</sup> Pb	<sup>207</sup> Pb/ <sup>206</sup> Pb	<sup>207</sup> Pb/ <sup>235</sup> U	<sup>206</sup> Pb/ <sup>238</sup> U	<sup>206</sup> Pb/ <sup>238</sup> U		<sup>207</sup> Pb/ <sup>235</sup> U	<sup>207</sup> Pb/ <sup>206</sup> Pb	
GU-13 (perovskite – dark brown fragments)															
1	3 N HCl corrected <sup>d</sup>	0.33	10.8	127	0.53	65.0	0.1265 ± 1	0.0508 ± 5	0.2746 ± 27	0.0391 ± 1	0.43	248 ± 1	246 ± 2	234 ± 21	
2	8 N HCl corrected <sup>d</sup>	0.80	2.72	37.5	0.44	69.4	0.1524 ± 1	0.0507 ± 7	0.2770 ± 43	0.0396 ± 2	0.44	250 ± 1	248 ± 4	229 ± 32	
3	6 N HCl corrected <sup>d</sup>	0.35	8.04	103	0.45	68.7	0.2008 ± 1	0.0513 ± 7	0.2797 ± 40	0.0395 ± 2	0.45	250 ± 1	250 ± 3	256 ± 30	
GU-28-41 (perovskite – dark brown fragments)															
4	8 N HCl corrected <sup>d</sup>	0.45	8.65	35.8	0.17	63.6	0.4783 ± 1	0.0509 ± 6	0.2772 ± 38	0.0395 ± 1	0.42	250 ± 1	248 ± 3	236 ± 29	
GU-08 (andradite – dark brown fragments)															
5	6 N HCl	1.15	0.43	7.01	0.32	112	0.2067 ± 1	0.0518 ± 3	0.2788 ± 19	0.0390 ± 1	0.42	247 ± 6	250 ± 2	278 ± 14	
6	6 N HCl	2.80	0.23	3.99	0.26	140	0.2397 ± 1	0.0517 ± 2	0.2397 ± 19	0.0389 ± 2	0.73	246 ± 1	249 ± 2	271 ± 11	

<sup>a</sup>All measured values are given to the last significant digit (based on the corresponding 2σ).

<sup>b</sup>Measured isotopic ratios.

<sup>c</sup>Rho represents correlation coefficients of <sup>207</sup>Pb/<sup>235</sup>U vs. <sup>206</sup>Pb/<sup>238</sup>U ratios.

<sup>d</sup>Pb<sub>c</sub> correction made using three-dimensional linear isochrons (Ludwig, 2003).

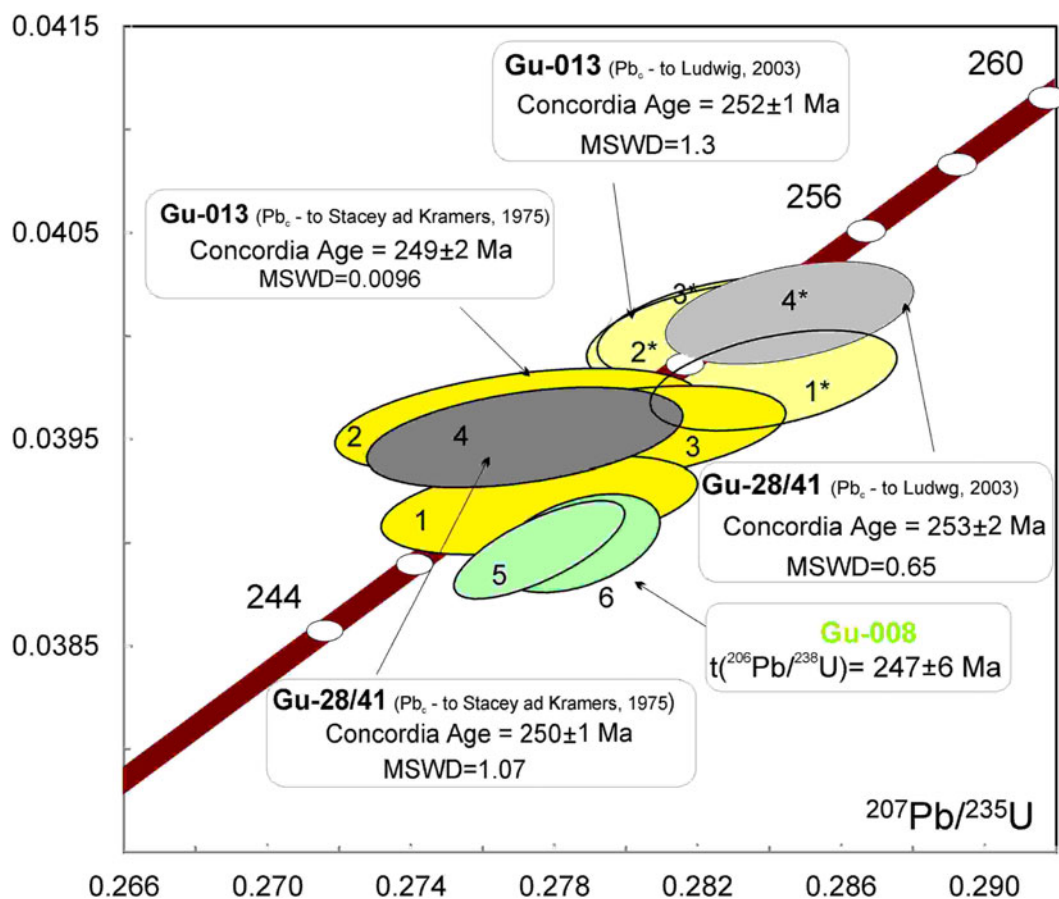


**Fig. 7.** U–Pb concordia diagram comparing ID-TIMS data for perovskite from jacupirangite (GU-28-41) and Northern carbonatite stock (GU-13) and andradite from the Southern stock (GU-08).

clearly desirable to provide robust constraints on the timing of this type of magmatism. Some mafic intrusions in the Angara–Taseevskaya depression (SW part of the Siberian flood basalt province) have been dated using U–Pb and <sup>40</sup>Ar–<sup>39</sup>Ar techniques to 254.2 ± 2.3– 255.8 ± 4.7/5.3 Ma (Paton *et al.*, 2010; Ivanov

*et al.*, 2013). The extent of this hypothetical earlier pulse of mantle activity is difficult to constrain because its manifestations were obviously obliterated by voluminous flood volcanism at ~252 Ma. It is important to note, however, that in other large igneous provinces, alkaline and carbonatitic magmatism was recurrent and

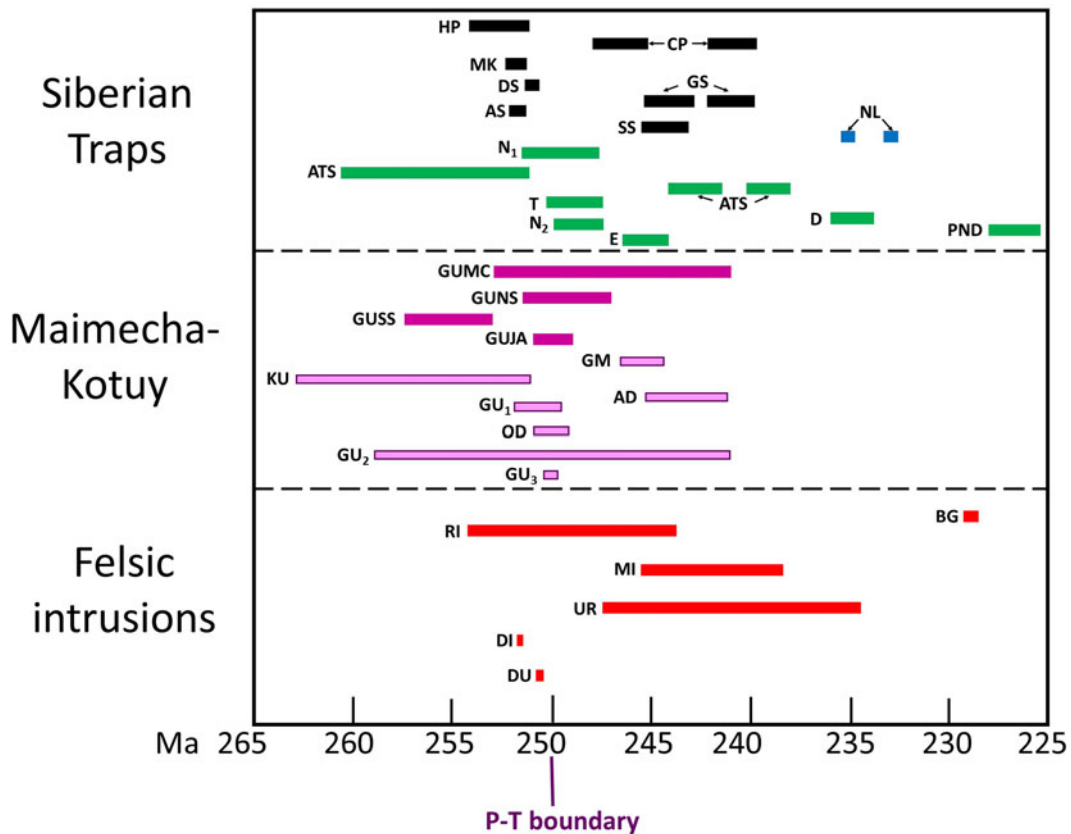


**Fig. 8.** Summary of geochronological data (from the literature and this work) for the Siberian flood basalts (black: lavas; green: intrusive rocks; blue: lamproites), Maimecha-Kotuy alkaline plutons (lilac: published data; purple: this work) and felsic intrusions (red). HP: Hoffman Peninsula (Reichow *et al.*, 2016); MK: Maimecha-Kotuy (Burgess and Bowring, 2015); CP, ATS and NL: central Putorana, Angara-Taseevskaya syncline and Noril'sk lamproite, respectively (Ivanov *et al.*, 2013, 2018); N<sub>1</sub>: Noril'sk intrusion (Renne, 1995); DS and AS: Delkansky and Arydzhangsky Suites (Kamo *et al.*, 2003); GS, SS, T, N<sub>2</sub>, E, PND and D: Gudchikhinsky suite, Syverminsky suite, Talnakh intrusion, Noril'sk vein, Ergalakhsky intrusion, Post-Norilsk dolerite dyke and Daldykansky intrusion (Dalrymple *et al.*, 1995); GUMC, GUSS, GUNS and GUJA: Guli melilitolite-carbonatite contact, Southern stock, Northern stock and jacupirangite (this work); GM and AD: Guli melilitolite and Avansky dyke (Dalrymple *et al.*, 1995); KU: Kugda (Anosova *et al.*, 2019); OD: Odikhincha (Salnikova *et al.*, 2019); GU<sub>1</sub>, GU<sub>2</sub>, GU<sub>3</sub>: Guli (Malich *et al.*, 2015; Kogarko and Zartman, 2007; Kamo *et al.*, 2003, respectively); BG: Bolgokhtokh granodiorite stock (Kamo *et al.*, 2003); RI, MI, UR: Uboinaya River, Morzhov Island, Rastorguev Island (Vernikovskiy *et al.*, 2003); DI and DU: Dikarabigai and Dumtalei intrusions (Augland *et al.*, 2019).

overlapping with the emplacement of tholeiitic rocks. For example, Cretaceous basaltic volcanism in the Paraná Basin of South America (133–135 Ma: Pinto *et al.*, 2011; Almeida *et al.*, 2018) was preceded, accompanied and followed by the emplacement of alkaline-ultramafic intrusions, many of which contain carbonatites (Eby and Mariano 1992; Gomes *et al.*, 1996; Antonini *et al.*, 2005; Speziale *et al.*, 2020). The oldest of these rocks predate the basalts by at least 6 Ma, whereas the youngest postdate them by some 15 Ma (Gomes *et al.*, 2013 and references therein). Hence, it is conceivable that the Siberian flood basalts, representing the world's largest igneous province, could also be preceded by small-volume mantle-derived magmas. The co-existence of carbonatites of different ages should also not be surprising, given the evidence of recurrent igneous activity at many structurally complex plutons, including carbonatite complexes (Guarino *et al.*, 2013, 2017; Poletti *et al.*, 2016).

Good agreement between the LA-ICPMS and ID-TIMS data for perovskite from the Northern carbonatite stock demonstrates that LA-ICPMS can be used reliably for *in situ* U–Pb age determination of compositionally heterogeneous perovskite (Figs. 2a–c, 3a–c). The main limitations of this type of analysis include a high proportion of common lead in this mineral ( $^{207}\text{Pb}/^{206}\text{Pb} = 0.85 \pm 0.02$ ) and the lack of a robust matrix-

matched standard. Considering matrix effects, we initially explored the possibility of using the Ice River perovskite as a calibration standard. However, several test runs showed that this material is not a reliable calibration standard at the analytical settings employed in the present work. The recommended age value of  $356.5 \pm 1.0$  Ma (Heaman, 2009) was determined for a single perovskite grain from the Ice River ijolite. A more recent study by Tappe and Simonetti (2012), based on multiple, smaller grains from ijolite and melteigite reported an appreciably older value of  $361.7 \pm 1.0$  Ma, and explained the discrepancy with Heaman's (2009) data by the presence of apatite inclusions in his material. These uncertainties compelled us to use zircon GJ-1 for calibration, even though it is not matrix-matched with respect to perovskite. The benefit of using zircon as a U–Pb standard is that it eliminates the need to correct calibration data for common Pb, which is an important potential source of errors with matrix-matched standards rich in common Pb. In this study, we demonstrate that LA-ICPMS analytical protocols can be modified by adjusting the laser focus, repetition rate and spray chamber configuration to effectively minimise any matrix effects. The use of a secondary, matrix-matched standard (e.g. Ice River perovskite) will further improve results by helping control the instrument mass bias. The Ice River perovskite cannot be recommended as

a calibration standard until the discrepancies between the original study by Heaman (2009) and that of Tappe and Simonetti (2012) have been addressed. In our opinion, it is important to examine multiple grains of perovskite from the Ice River ijolite to verify its isotopic homogeneity, because it is not unusual for alkaline rocks to contain more than one generation of perovskite representing distinct and temporally disconnected evolutionary processes (Chakhmouradian and Mitchell, 2001; Zurevinski *et al.*, 2011; Ranger *et al.*, 2018; Tappe *et al.*, 2018).

**Acknowledgements.** This work was supported by the Natural Sciences and Engineering Research Council of Canada (Discovery Grant to ARC). We are grateful to Marina Sevastyanova, Mikhail Martyshkin and Ivan Kalmykov (Polyarnaya Exploration Company) for their hospitality while in Khatanga, as well as their generous help with fieldwork logistics. Larry M. Heaman is thanked for donating the Ice River perovskite. The manuscript has benefited from constructive reviews by Sebastian Tappe and an anonymous reviewer.

## References

- Afanasenkov A.P., Nikishin A.M., Unger A.V., Bordunov S.I., Lugovaya O.V., Chikishev A.A. and Yakovishina E.V. (2016) The tectonics and stages of the geological history of the Yenisei-Khatanga Basin and the conjugate Taimyr Orogen. *Geotectonics*, **50**, 161–178.
- Almeida V.V., Janasi V.A., Heaman L.M., Shaulis B.J., Hollanda M.H.B.M. and Renne P.R. (2018) Contemporaneous alkaline and tholeiitic Magmatism in the Ponta Grossa Arch, Paraná-Etendeka Magmatic Province: Constraints from U–Pb zircon/baddeleyite and  $^{40}\text{Ar}/^{39}\text{Ar}$  phlogopite dating of the José Fernandes Gabbro and Mafic dykes. *Journal of Volcanology and Geothermal Research*, **355**, 55–65.
- Anosova M.O., Kostitsyn Yu.A. and Kogarko L.N. (2019) Correlation of high-calcium silica-undersaturated complex of the Maymecha–Kotuy Province with Siberian Flood Basalts: new age data on the Kudga Massif (Polar Siberia). *Geochemistry International*, **57**, 1339–1342.
- Antonini P., Gasparon M., Comin-Chiaramonti P. and Gomes C.B. (2005) Post Palaeozoic Magmatism in the Eastern Paraguay: Sr–Nd–Pb isotope compositions. Pp. 57–70 in: *Mesozoic to Cenozoic Alkaline Magmatism in the Brazilian Platform* (P. Comin-Chiaramonti and C.B. Gomes, editors). Edusp/Fapesp, São Paulo, Brazil.
- Augland L. E., Ryabov V.V., Vernikovsky V.A., Planke S., Polozov A.G., Callegaro S., Jerram D.A. and Svensen H.H. (2019) The Main pulse of the Siberian Traps expanded in size and composition. *Scientific Reports*, **9**, 18723.
- Batumike J.M., Griffin W.L., Belousova E., Pearson N.J., O'Reilly S.Y. and Shee S. (2008) LAM-ICPMS U–Pb dating of kimberlitic perovskite: Eocene–Oligocene kimberlites from the Kundelungu Plateau, D.R. Congo. *Earth and Planetary Science Letters*, **267**, 609–619.
- Burgess S.D. and Bowring S.A. (2015) High-precision geochronology confirms voluminous Magmatism before, during, and after Earth's most severe extinction. *Science Advances*, **1**, e1500470.
- Castillo-Oliver M., Galí S., Melgarejo J.C., Griffin W.L., Belousova E., Pearson N.J., Watangua M. and O'Reilly S.Y. (2016) Trace-element geochemistry and U–Pb dating of perovskite in kimberlites of the Lunda Norte province (NE Angola): Petrogenetic and tectonic implications. *Chemical Geology*, **426**, 118–134.
- Chakhmouradian A.R. and Mitchell R.H. (1997) Compositional variation of perovskite-group minerals from the carbonate complexes of the Kola Alkaline Province, Russia. *The Canadian Mineralogist*, **35**, 1293–310.
- Chakhmouradian A.R. and Mitchell R.H. (2000) Occurrence, compositional variation and alteration of perovskite in kimberlites. *The Canadian Mineralogist*, **38**, 975–994.
- Chakhmouradian A.R. and Mitchell R.H. (2001) Three compositional varieties of perovskite from kimberlites of the Lac de Gras field (Northwest Territories, Canada). *Mineralogical Magazine*, **65**, 133–148.
- Chakhmouradian A.R., Reguir E.P., Vadim S. Kamenetsky V.S., Sharygin V.V. and Golovin A.V. (2013) Trace-element partitioning in perovskite: Implications for the geochemistry of kimberlites and other mantle-derived undersaturated rocks. *Chemical Geology*, **353**, 112–131.
- Corfu F. and Andersen T.B. (2002) U–Pb ages of the Dalsfjord Complex, SW Norway and their bearing on the correlation of allochthonous crystalline segment of the Scandinavian Caledonides. *International Journal of Earth Science*, **91**, 955–963.
- Cox R.A. and Wilton D.H.C. (2006) U–Pb dating of perovskite by LA-ICPMS: an example from the Oka carbonatite, Quebec, Canada. *Chemical Geology*, **235**, 21–32.
- Dalrymple G.B., Czamanske J.G.K., Fedorenko V.A., Simonov O.N., Lanphere M.A. and Likhachev A.P. (1995) A reconnaissance  $^{40}\text{Ar}/^{39}\text{Ar}$  geochronologic study of ore-bearing and related rocks, Siberian Russia. *Geochimica et Cosmochimica Acta*, **59**, 2071–2083.
- Deng X.D., Li J.W., Luo T. and Wang H.Q. (2017) Dating Magmatic and hydrothermal processes using andradite-rich garnet U–Pb geochronometry. *Contributions to Mineralogy and Petrology*, **172**, 71.
- DeWolf C.P., Zeissler C.J., Halliday A.N., Mezger K. and Essene E.J. (1996) The role of inclusions in U–Pb and Sm–Nd garnet geochronology: Stepwise dissolution experiments and trace uranium Mapping by fission track analysis. *Geochimica et Cosmochimica Acta*, **60**, 121–134.
- Donnelly C.L., Griffin W.L., Yang J.-H., O'Reilly S.Y., Li Q.-L., Parson N.J. and Li X.-H. (2012) In situ U–Pb dating and Sr–Nd isotopic analysis of perovskite: constraints on the age and petrogenesis of the Kuruman Kimberlite Province, Kaapvaal Craton, South Africa. *Journal of Petrology*, **53**, 2497–2522.
- Eby G. and Mariano A. (1992) Geology and geochronology of carbonatites and associated alkaline rocks peripheral to the Paraná Basin, Brazil-Paraguay. *Journal of South American Earth Sciences*, **6**, 207–216.
- Frei D. and Gerdes A. (2009) Precise and accurate in situ U–Pb dating of zircon with high sample throughput by automated LA-SF-ICP-MS. *Chemical Geology*, **261**, 261–270.
- Gomes C.B., Comin-Chiaramonti P., Velázquez V.F. and Orué D. (1996) Alkaline Magmatism in Paraguay: a review. Pp. 31–56 in: *Mesozoic to Cenozoic Alkaline Magmatism in the Brazilian Platform* (P. Comin-Chiaramonti and C.B. Gomes, editors). Edusp/Fapesp, São Paulo, Brazil.
- Gomes C.B., Comin-Chiaramonti P. and Velázquez V.F. (2013) Synthesis on the alkaline Magmatism of Eastern Paraguay. *Brazilian Journal of Geology*, **43**, 745–61.
- Guarino V., Wu F.-Y., Lustrino M., Melluso L., Brotzu P., Gomes C.B., Ruberti E., Tassinari C.C.G. and Svisero D.P. (2013) U–Pb ages, Sr–Nd isotope geochemistry, and petrogenesis of kimberlites, kamafugites and phlogopite-picroites of the Alto Paranaíba Igneous Province, Brazil. *Chemical Geology*, **353**, 65–82.
- Guarino V., Wu F.-Y., Melluso L., de Barros Gomes C., Tassinari C.C.G., Ruberti E. and Brilli M. (2017) U–Pb ages, geochemistry, C–O–Nd–Sr–Hf isotopes and petrogenesis of the Catalão II carbonatitic complex (Alto Paranaíba Igneous Province, Brazil): implications for regional-scale heterogeneities in the Brazilian carbonatite associations. *International Journal of Earth Sciences*, **106**, 1963–1989.
- Hamilton M.A., Sobolev N.V., Stern R.A. and Pearson D.G. (2003) SHRIMP U–Pb dating of a perovskite inclusion in diamond: evidence for a syneruptive age for diamond formation, Sytkanskaya kimberlite pipe, Yakutia region, Siberia. *Extended Abstract 8th International Kimberlite Conference*, FLA\_0388.
- Heaman L.M. (1989) The nature of the subcontinental Mantle from Sr–Nd–Pb isotopic studies on kimberlitic perovskite. *Earth and Planetary Science Letters*, **92**, 323–334.
- Heaman L.M. (2009) The application of U–Pb geochronology to Mafic, ultramafic and alkaline rocks: An evaluation of three mineral standards. *Chemical Geology*, **261**, 43–52.
- Heaman L.M., Pell J., Grütter H.S. and Creaser R.A. (2015) U–Pb geochronology and Sr/Nd isotope compositions of groundmass perovskite from the newly discovered Jurassic Chidliak kimberlite field. *Earth and Planetary Science Letters*, **415**, 183–199.
- Heaman L.M., Phillips D. and Pearson D.G. (2019) Dating kimberlites: methods and emplacement patterns through time. *Elements*, **15**, 399–404.
- Horwitz E.P., Dietz M.L., Chiarizia R., Diamond H., Essling A.M. and Graczyk D. (1992) Separation and preconcentration of uranium from

- acidic media by extraction chromatography. *Analitica Chimica Acta*, **266**, 25–37.
- Ireland T.R., Compston W., Williams I.S. and Wendt I. (1990) U–Th–Pb systematics of individual perovskite grains from the Allende and Murchison carbonaceous chondrites. *Earth and Planetary Science Letters*, **101**, 379–387.
- Ivanov A.V., He H., Yan L., Ryabov V.V., Shevko A.Y., Palesskii S.V. and Nikolaeva I.V. (2013) Siberian Traps large igneous province: Evidence for two flood basalt pulses around the Permo-Triassic boundary and in the Middle Triassic, and contemporaneous granitic magmatism. *Earth-Science Reviews*, **122**, 58–76.
- Ivanov A.V., Demonterova E.I., Savatenkov V.M., Perepelov A.B., Ryabov V.V. and Shevko A.Y. (2018) Late Triassic (Carnian) lamproites from Noril'sk, polar Siberia: Evidence for melting of the recycled Archean crust and the question of lamproite source for some placer diamond deposits of the Siberian Craton. *Lithos*, **296–299**, 67–78.
- Jackson S.E., Pearson N.J., Griffin W.L. and Belousova E.A. (2004) The application of laser ablation-inductively coupled plasma-mass spectrometry to in situ U–Pb zircon geochronology. *Chemical Geology*, **211**, 47–69.
- Kamo S.L., Czamanske G.K., Amelin Y., Fedorenko V.A., Davis D.W. and Trofimov V.R. (2003) Rapid eruption of Siberian flood-volcanic rocks and evidence for coincidence with the Permian-Triassic boundary and Mass extinction at 251 Ma. *Earth and Planetary Science Letters*, **214**, 75–91.
- Kinny P.D., Griffin B.J., Heaman L.M., Brakhfogel F.F. and Spetsius Z.V. (1997) SHRIMP U–Pb ages of perovskite from Yakutian kimberlites. *Russian Geology and Geophysics*, **38**, 97–105.
- Kogarko L.N. and Zartman R.E. (2007) A Pb isotope investigation of the Guli Massif, Maymecha-Kotuy alkaline-ultramafic complex, Siberian flood basalt province, Polar Siberia. *Mineralogy and Petrology*, **89**, 113–132.
- Krogh T.E. (1973) A low-contamination method for hydrothermal decomposition of zircon and extraction of U and Pb for isotopic age determination. *Geochimica et Cosmochimica Acta*, **37**, 485–494.
- Kuhn H.-R. and Günther D. (2003) Elemental fractionation studies in Laser Ablation Inductively Coupled Plasma Mass Spectrometry on Laser-Induced Brass Aerosols. *Analytical Chemistry*, **75**, 747–753.
- Le Maitre R.W. (2002) *Igneous rocks: a Classification and Glossary of Terms. Recommendations of the International Union of Geological Sciences, Sub-Commission on the Systematics of Igneous Rocks*. Cambridge University Press, UK.
- Li Q.-L., Li X.H., Liu Y., Wu F.-Y., Yanga J.-H. and Mitchell R.H. (2010) Precise U–Pb and Th–Pb age determination of kimberlitic perovskites by secondary ion Mass spectrometry. *Chemical Geology*, **269**, 396–405.
- Ludwig K.R. (1991) PbDat for MS-DOS, version 1.21 U.S. Geological Survey Open-File Report, 88.
- Ludwig K.R. (2003) Isoplot 3.70. A Geochronological Toolkit for Microsoft Excel. *Berkeley Geochronology Center Special Publications*, **4**.
- Ludwig K.R. (2012) Isoplot 3.75. A geochronological toolkit for Microsoft Excel. *Berkeley Geochronology Center Special Publications*, **5**.
- Malich K.N., Khiller V.V., Badanina I.Y. and Belousova E.A. (2015) Results of dating of thorianite and baddeleyite from carbonatites of the Guli Massif, Russia. *Doklady Earth Sciences*, **464**, 1029–1032.
- Malitch K.N., Efimov A.A. and Badanina I.Yu. (2011) Contrasting platinum-group mineral assemblages from chromitites of the Nizhny Tagil and Guli Massifs (Russia): implications for composition, sources and age. *Doklady Earth Sciences*, **441**, 1514–1518.
- Paton C., Hergt J.M., Phillips D., Woodhead J.D. and Shee S.R. (2007) New insights into the genesis of Indian kimberlites from the Dharwar Craton via in-situ Sr-isotope analysis of groundmass perovskite. *Geology*, **35**, 1011–1014.
- Paton M.T., Ivanov A.V., Fiorentini M.L., McNaughton M.J., Mudrovska I., Reznitskii L.Z. and Demonterova E.I. (2010) Late Permian and Early Triassic Magmatic pulses in the Angara-Taseeva syncline, Southern Siberian Traps and their possible influence on the environment. *Russian Geology and Geophysics*, **51**, 1012–1020.
- Paton C., Hellstrom J., Paul B., Woodhead J. and Hergt J. (2011) Iolite: free-ware for the visualisation and processing of Mass spectrometric data. *Journal of Analytical Atomic Spectrometry*, **26**, 2508–2518.
- Petrus J.A. and Kamber B.S. (2012) VizualAge: a novel approach to laser ablation ICPMS U–Pb geochronology data reduction. *Journal of Geostandards and Geoanalytical Research*, **36**, 247–270.
- Pinto V.M., Hartmann L.A., Santos J.O.S., McNaughton N.J. and Wildner W. (2011) Zircon U–Pb geochronology from the Paraná bimodal volcanic province support a brief eruptive cycle at ~135 Ma. *Chemical Geology*, **281**, 93–102.
- Poletti J.E., Cottle J.M., Hagen-Peter G.A. and Lackey J.S. (2016) Petrochronological Constraints on the Origin of the Mountain Pass Ultrapotassic and Carbonatite Intrusive Suite, California. *Journal of Petrology*, **57**, 1555–1598.
- Ranger I.M., Heaman L.M., Pearson D.G., Muntener C. and Zhuk V. (2018) Punctuated, long-lived emplacement history of the Renard 2 kimberlite, Canada, revealed by new high precision U–Pb groundmass perovskite dating. *Mineralogy and Petrology*, **112**, 639–651.
- Rass I.T. and Dubrovinskii L.S. (1997) The schorlomite thermodynamic parameters and stability field. *Doklady RAS*, **354**, 191–198.
- Reguir E.P., Camacho A., Yang P., Chakhmouradian A.R., Kamenetsky V.S. and Halden N.M. (2010) Trace-element study and uranium-lead dating of perovskite from the Afrikanda plutonic complex, Kola Peninsula (Russia) using LA-ICP-MS. *Mineralogy and Petrology*, **100**, 95–103.
- Reichow M.K., Saunders A.D., Scott R.A., Millar I.L., Barfod D., Pringle M.S., Rogers N.W. and Hammond S. (2016) Petrogenesis and timing of Mafic Magmatism, South Taimyr, Arctic Siberia: A northerly continuation of the Siberian Traps? *Lithos*, **248–251**, 382–401.
- Renne P.R. (1995) Excess <sup>40</sup>Ar in biotite and hornblende from the Noril'sk 1 intrusion, Siberia: implications for the age of the Siberian Traps. *Earth and Planetary Science Letters*, **131**, 165–176.
- Salnikova E.B., Stifeeva M.V., Nikiforov A.V., Yarmolyuk V.V., Kotov A.B., Anisimova I.V., Sugorakova A.M. and Vrublevskii V.V. (2018) Andradite–morimotoite garnets as promising U–Pb geochronometers for dating ultrabasic alkaline rocks. *Doklady Earth Sciences*, **480**, 779–783.
- Salnikova E.B., Chakhmouradian A.R., Stifeeva M.V., Reguir E.P., Kotov A.B., Gritsenko Yu.D. and Nikiforov A.V. (2019) Calcic garnets as a geochronological and petrogenetic tool applicable to a wide variety of rocks. *Lithos*, **338–339**, 141–154.
- Smith C.B., Allsopp H.I., Gravie O.G., Kramers J.D., Jackson P.F.S. and Clement C.R. (1989). Note on the U–Pb perovskite method for dating kimberlites: examples from Wesselton and De Beers mines, South Africa and Somerset Island, Canada. *Chemical Geology. Isotope Geoscience Section*, **79**, 137–145.
- Speziale S., Castorina F., Censi P., de Barros Gomes C., Soares Marques L. and Comin-Chiaromonte P. (2020) Carbonatites from the Southern Brazilian platform: I. *Open Geosciences*, **12**, 452–478.
- Srivastava R.K., Heaman L.M., Singha A. and Shihua S. (2005) Emplacement age and isotope geochemistry of Sung Valley alkaline-carbonatite complex, Shillong Plateau, northeastern India: Implications for primary carbonate melt and genesis of the associated silicate rocks. *Lithos*, **81**, 33–54.
- Stacey J.S. and Kramers J.D. (1975) Approximation of terrestrial lead isotope evolution by a two-stage model. *Earth and Planetary Science Letters*, **26**, 207–221.
- Stamm N., Schmidt M.W., Szymanowski D., von Quadt A., Mohapi T. and Fourie A. (2018) Primary petrology, mineralogy and age of the Letšeng-la-Terae kimberlite (Lesotho, Southern Africa) and parental Magmas of Group-I kimberlites. *Contributions to Mineralogy and Petrology*, **173**, 76.
- Steiger R.H. and Jäger E. (1977) Subcommittee on geochronology: convention on the use of decay constants in geo- and cosmochronology. *Earth and Planetary Science Letters*, **36**, 359–362.
- Stifeeva, M.V., Salnikova, E.B., Arzamastsev, A.A., Kotov, A.B. and Grozdev, V.Yu. (2020) Calcic garnets as a source of information on the age of ultramafic alkaline intrusions in the Kola Magmatic Province. *Petrology*, **28**, 72–84.
- Tappe S. and Simonetti A. (2012) Combined U–Pb geochronology and Sr–Nd isotope analysis of the Ice River perovskite standard, with implications for kimberlite and alkaline rock petrogenesis. *Chemical Geology*, **304–305**, 10–17.
- Tappe S., Foley S.F., Jenner G.A., Heaman L.M., Kjarsgaard B.A., Romer R.L., Stracke A., Joyce N. and Hoefs J. (2006) Genesis of ultramafic lamprophyres and carbonatites at Aillik Bay, Labrador: a consequence of incipient

- lithospheric thinning beneath the North Atlantic Craton. *Journal of Petrology*, **47**, 1261–1315.
- Tappe S., Dongre A., Liu C.-Z. and Wu F.-Y. (2018) 'Premier' evidence for prolonged kimberlite pipe formation and its influence on diamond transport from deep Earth. *Geology*, **46**, 843–846.
- Tera F. and Wasserburg G.J. (1972) U-Th-Pb systematics in three Apollo 14 basalts and the problem of initial Pb in lunar rocks. *Earth and Planetary Science Letters*, **14**, 281–304.
- Vernikovskiy V.A., Pease V.L., Vernikovskaya A.E., Romanov A.P., Gee D.G. and Travin A.V. (2003) First report of early Triassic A-type granite and syenite intrusions from Taimyr: product of the northern Eurasian superplume? *Lithos*, **66**, 23–36.
- Wiedenbeck M., Hancher J.M., Peck W.H., Sylvester P., Valley J., Whitehouse M., Kronz A., Morishita Yu., Nasdala L., Fiebig J., Franchi I., Girard J.-P., Greenwood R.C., Hinton R., Kita N., Mason P.R.D., Norman M., Ogasawara M., Piccoli P.M., Rhede D., Satoh H., Schulz-Dobrick B., Skår Ø., Spicuzza M.J., Terada K., Tindle A., Togashi S., Vennemann T., Xie Q. and Zheng Y.-F. (2002) Further characterisation of the 91500 zircon crystal. *Geostandards and Geoanalytical Research*, **28**, 9–39.
- Yang Y.H., Wu F.Y., Yang J.H., Mitchell R.H., Zhao Z.F., Xie L.W., Huang C., Ma Q., Yang M. and Zhao H. (2018) U–Pb age determination of schorlomite garnet by laser ablation inductively coupled plasma Mass spectrometry. *Journal of Analytical Atomic Spectrometry*, **33**, 231–239.
- Yegorov L.S. (1969) *The Melilitic Rocks of the Maimecha-Kotui Province*. Nedra Press, Leningrad, USSR [in Russian].
- Yegorov L.S. (1989) The shape, structure and evolution of the Guli Massif of ultramafic-alkaline rocks and carbonatites. *Izvestiya Akademii Nauk SSSR, Geological Series*, **7**, 41–56 [in Russian].
- Yegorov L.S. (1991) *Ijolite Carbonatite Plutonism (Example of the Maimecha-Kotui Complex of Northern Siberia)*. Nedra Press, Leningrad, USSR [in Russian].
- Yeliseev N.A. and Sheinmann Yu.M. (editors) (1961) *The Guli Intrusion of Ultramafic-Alkaline Rocks*. Gosgortekhizdat, Moscow, 274 pp. [in Russian].
- Zurevinski S., Heaman L.M. and Creaser R.A. (2011) The origin of Triassic/Jurassic kimberlitic Magmatism, Canada: Two Mantle sources revealed from the Sr–Nd isotopic composition of groundmass perovskite. *Geochemistry Geophysics Geosystems*, **12**, article 9.